
Isospin analysis and study of the decay modes

$$\bar{B}^0 \rightarrow \Lambda_c^+ \bar{p} \pi^0 \text{ and } \bar{B}^0 \rightarrow \Lambda_c^+ \bar{p} \eta$$

DISSERTATION

zur Erlangung des akademischen Grades
Doctor rerum naturalium (Dr. rer. nat.)
der Mathematisch-Naturwissenschaftlichen Fakultät
der Universität Rostock

vorgelegt von Diplom-Physiker Marcus Ebert
geboren am 6. September 1975
in Wolfen

Gutachter

Priv.-Doz. Dr. Roland Waldi
Institut für Physik
Universität Rostock
Universitätsplatz 3
18055 Rostock
Germany

Prof. Dr. Heiko Lacker
Institut für Physik
Humboldt-Universität zu Berlin
Newtonstraße 15
12489 Berlin
Germany

eingereicht am: 01. April 2011
verteidigt am: 31. Mai 2011

Abstract

In this thesis the analyses of the decays $\bar{B}^0 \rightarrow \Lambda_c^+ \bar{p} \pi^0$ and $\bar{B}^0 \rightarrow \Lambda_c^+ \bar{p} \eta$, including all possible two-body invariant mass distributions, is presented. The analyses are based on a data sample of about 467 million $B\bar{B}$ pairs collected with the *BABAR* detector at the PEP-II collider at SLAC. The decay $\bar{B}^0 \rightarrow \Lambda_c^+ \bar{p} \pi^0$ is observed for the first time, the branching fraction calculated and an enhancement at the threshold of the invariant mass of the baryon-antibaryon pair is observed. Evidence for the decay $\bar{B}^0 \rightarrow \Lambda_c^+ \bar{p} \eta$ was found, too. For this decay mode no enhancement at the threshold of the invariant mass of the baryon-antibaryon pair is seen. Both decay modes are compared with the similar decay $B^- \rightarrow \Lambda_c^+ \bar{p} \pi^-$ using isospin relations and it is studied if the weak decay prefers one of the possible isospins of the final state. Using the results, predictions for the branching fraction of other baryonic B -decay modes are given.

Kurzfassung

In dieser Arbeit werden die Analysen der Zerfälle $\bar{B}^0 \rightarrow \Lambda_c^+ \bar{p} \pi^0$ und $\bar{B}^0 \rightarrow \Lambda_c^+ \bar{p} \eta$, inklusive der möglichen Zweikörpermassenverteilungen, vorgestellt. Die Arbeit basiert auf einem Datensample von ungefähr 467 Millionen $B\bar{B}$ Paaren, welche mit dem *BABAR* -Detektor am PEP-II Speicherring am SLAC aufgezeichnet wurden. Der Zerfall $\bar{B}^0 \rightarrow \Lambda_c^+ \bar{p} \pi^0$ wurde zum ersten Mal beobachtet und das Verzweigungsverhältnis bestimmt. Für diesen Zerfallskanal wurde eine Anhäufung von Signalereignissen bei sehr kleinen Werten für $m(\Lambda_c^+ \bar{p})$ gefunden. Evidenz für den Zerfall $\bar{B}^0 \rightarrow \Lambda_c^+ \bar{p} \eta$ wurde ebenfalls gefunden, allerdings keine Anhäufung von Ereignissen bei kleinen Werten für $m(\Lambda_c^+ \bar{p})$. Beide Zerfälle wurden mit dem ähnlichen Zerfall $B^- \rightarrow \Lambda_c^+ \bar{p} \pi^-$ verglichen. Dazu wurden Isospinrelationen verwendet und es wurde untersucht, ob der schwache Zerfall einen der möglichen Isospins für den Endzustand bevorzugt. Die gefundenen Resultate wurde dazu verwendet Vorhersagen für das Verzweigungsverhältnis anderer baryonischer B -Zerfälle zu machen.

Contents

1	Introduction to Elementary Particle Physics	1
1.1	The Standard Model of Elementary Particle Physics	1
1.1.1	Elementary Particles	1
1.1.1.1	Electro-Magnetic Interaction	2
1.2	First look at the analyzed decay modes	5
1.2.1	Comparison of different decay modes	6
2	The <i>BABAR</i> Experiment	11
2.1	The <i>BABAR</i> detector	13
2.1.1	Silicon Vertex Detector (SVT)	14
2.1.2	Tracking Chamber (DCH)	14
2.1.3	Cherenkov Detector (DIRC)	15
2.1.4	Electron and Photon Detector (EMC)	15
2.1.5	Magnet Coil	17
2.1.6	Muon and Hadron Detector	17
2.2	<i>BABAR</i> Framework	18
2.2.1	Trigger System and Track Reconstruction	18
2.2.2	Charged Particle Identification using Likelihood Selectors	18
3	Decay reconstruction	21
3.1	Event characteristics for B reconstruction at <i>BABAR</i>	21
3.2	Simulated Events	22
3.3	Reconstruction of $\bar{B}^0 \rightarrow \Lambda_c^+ \bar{p} \pi^0$	22
3.3.1	Selection criteria	24
3.3.2	Peaking background	25
3.3.3	Continuum Background	28
3.3.4	Calculation of the branching fraction	31
3.3.4.1	Efficiency determination	31
3.3.4.2	Determination of the number of produced signal events	34
3.3.4.3	Branching fraction calculation	35
3.3.5	Cross checks	35
3.3.6	Resonances	37
3.3.6.1	$\Lambda_c^+ \pi^0$ resonant states	37
3.3.6.2	$\Lambda_c^+ \bar{p}$ mass distribution	39
3.3.7	Systematic uncertainties	40
3.4	Reconstruction of $\bar{B}^0 \rightarrow \Lambda_c^+ \bar{p} \eta$	41
3.4.1	Selection Criteria	41
3.4.2	Calculation of the branching fraction	42
3.4.2.1	Efficiency determination	44

3.4.2.2	Determination of the number of produced signal events	44
3.4.2.3	Branching fraction calculation	45
3.4.3	Cross checks	46
3.4.4	Two-body mass distributions	46
3.4.5	Systematic uncertainties	47
4	Results and Conclusions	51
4.1	Comparison of branching fractions	51
4.1.1	Measured branching fractions	51
4.1.2	Ratio of branching fractions	52
4.1.3	Predictions	53
4.2	Conclusion and Outlook	54
	Bibliography	55

List of Figures

1.1	Electron-electron scattering in the electro-magnetic interaction	3
1.2	Electron-positron annihilation to a virtual photon and creation of a $b\bar{b}$ quark pair in the electro-magnetic interaction	3
1.3	Neutron decay in the model of exchange particles.	4
1.4	Possibilities of gluon exchange between the quarks of a pion.	4
1.5	Decay of $\Upsilon(4S)$ to two neutral B mesons.	5
1.6	Feynman diagrams which are similar for the decay of the \bar{B}^0 (left) and the B^- (right).	7
1.7	Feynman diagram where the quarks from the W^- decay are combined to a π^- which is only possible for the decay of the B^-	8
1.8	Feynman diagram where the W^- interacts with the \bar{d} from the \bar{B}^0 which is only possible for the decay of the \bar{B}^0	8
1.9	Feynman diagram where the $q\bar{q}$ ($s\bar{s}$) is created out of gluons and make the η	8
2.1	Graphics of the linear accelerator and PEP-II collider together with some basic facts, like the beam energies.	11
2.2	Recorded luminosity during the lifetime of the <i>BABAR</i> experiment. . .	12
2.3	Schematic view of the constituent parts of the <i>BABAR</i> detector.	13
2.4	One half of the SVT seen from the inside direction.	14
2.5	The DCH with all wires in it.	15
2.6	View of the photomultiplier tubes installed in the DIRC.	16
2.7	Schematic view how the crystals of the EMC are arranged in the r-z-plane (left) and x-y-plane (right).	17
2.8	Energy loss as a function of the momentum $p = mv$	19
3.1	m_{ES} distributions for different MC channels (Run1-5 MC), distribution on the top is for signal MC; red data points = after veto cuts . .	26
3.2	$m_{ES}:\Delta E$ distributions for different MC channels before veto cuts applied (Run1-5 MC)	27

3.3	Red points are onpeak data, shaded histogram shows scaled offpeak data (before the thrust-cut).	29
3.4	Thrust distribution for signal MC (red) and $c\bar{c}$ MC (black); the blue dashed line shows the cut value	29
3.5	Red points are onpeak data, shaded histogram shows scaled offpeak data (after the thrust-cut).	30
3.6	Black points are onpeak data; magenta histogram = scaled $B^0\bar{B}^0$ MC; blue histogram = scaled B^+B^- MC; green histogram = scaled $c\bar{c}$ MC; red histogram = scaled uds MC	30
3.7	Fitted m_{ES} distribution without efficiency correction (data points); the result of the fit (solid line) and the background estimate (dashed line) is shown.	32
3.8	Shaded histogram shows scaled signal MC; black points are sideband subtracted data for $m_{ES} > 5.272 \text{ GeV}/c^2$; scaled to the same integral.	33
3.9	Shaded histogram shows scaled signal MC; black data points for sideband subtracted data with $m_{ES} > 5.272 \text{ GeV}/c^2$; scaled to the same integral.	33
3.10	data points are for sideband subtracted signal events in data; shaded histogram shows scaled signal MC.	34
3.11	efficiency distribution fitted with a 4th order polynomial	34
3.12	Efficiency-corrected m_{ES} distribution for $\bar{B}^0 \rightarrow \Lambda_c^+ \bar{p} \pi^0$ (data points). The result of the fit (solid line) and the background estimate (dashed line) is shown.	35
3.13	distribution of sideband subtracted data events fitted with a Crystal Ball function; blue lines show the cuts on $m(\gamma\gamma)$ for the default analysis.	36
3.14	distribution of sideband subtracted data events fitted with a Gaussian; blue lines show the cuts on $m(pK^-\pi^+)$ for the default analysis.	37
3.15	Distribution of the invariant mass of the $\Lambda_c^+ \pi^0$ system in the region where the $\Sigma_c^+(2455)$ resonance is expected; points are for data within the m_{ES} signal region, the curve shows the fit.	38
3.16	Likelihood distribution for the number of signal events from the fit in fig. 3.15	38
3.17	Efficiency corrected distribution of the invariant mass $m(\Lambda_c^+ \bar{p})$; points are signal data events; histogram shows signal MC events assuming a phase space distribution normalized to the number of data events.	39
3.18	ΔE distribution for data signal events after all selection cuts (data points) and signal MC events (histogram) normalized to the number of data signal events; signal events are obtained from binwise m_{ES} fits; dashed lines show the range used for m_{ES} distributions.	40
3.19	Black points are onpeak data; magenta histogram = scaled $B^0\bar{B}^0$ MC; blue histogram = scaled B^+B^- MC; green histogram = scaled $c\bar{c}$ MC; red histogram = scaled uds MC	43

-
- 3.20 Fitted m_{ES} distribution without efficiency correction (data points); the result of the fit (solid line) and the background estimate (dashed line) is shown. 43
- 3.21 Efficiency distribution in bins of $m(\Lambda_c^+ \bar{p})$ fitted with a 4th order polynomial. 44
- 3.22 Efficiency-corrected m_{ES} distribution ; the result of the fit (solid line) and the background estimate are shown. 45
- 3.23 Distribution of sideband subtracted data events fitted with a Novosibirsk function $f \sim e^{-\frac{1}{2} \left(\frac{\ln^2 [1 + \Lambda \tau \cdot (m(\gamma\gamma) - \mu)]}{\tau^2} + \tau^2 \right)}$ and $\Lambda = \sinh(\tau \sqrt{\ln 4}) / (\sigma \tau \sqrt{\ln 4})$ where μ is the mean, σ the width and τ the asymmetry of this function; blue lines show the cut range for $m(\gamma\gamma)$ 46
- 3.24 Distribution of sideband subtracted data events fitted with a Gaussian. 47
- 3.25 Efficiency corrected distribution of sideband subtracted signal data events (data points) and phase space generated MC signal events (histogram) for $m(\bar{p}\eta)$; scaled to the same integral. 48
- 3.26 Efficiency corrected distribution of sideband subtracted signal data events (data points) and phase space generated MC signal events (histogram) for $m(\Lambda_c^+ \bar{p})$; scaled to the same integral. 48
- 3.27 Efficiency corrected distribution of sideband subtracted signal data events (data points) and phase space generated MC signal events (histogram) for $m(\Lambda_c^+ \eta)$; scaled to the same integral. 49

List of Tables

1.1	Particles of the standard model of elementary particle physics and the exchange particles of the electro-weak interaction.	1
1.2	Clebsch-Gordon-Coefficients squared for the different decays	9
2.1	Usable data luminosity and number of $B\bar{B}$ pairs of the different time periods.	12
2.2	Definition of the variables in the Bethe-Bloch-Formula	20
3.1	Simulated B decay modes used in the analysis.	22
3.2	Simulated inclusive MC modes used for background studies in the analysis.	23
3.3	fixed parameters of the signal fitting function obtained from MC signal events	31
3.4	fixed parameters of the signal fitting function obtained from efficiency corrected MC signal events	35
3.5	Systematic uncertainties for the reconstruction of $\bar{B}^0 \rightarrow \Lambda_c^+ \bar{p} \pi^0$	41
3.6	fixed parameters of the signal fitting function obtained from MC signal events	44
3.7	fixed parameters of the signal fitting function obtained from efficiency corrected MC signal events	45
3.8	Systematic uncertainties for the reconstruction of $\bar{B}^0 \rightarrow \Lambda_c^+ \bar{p} \eta$	47

1. Introduction to Elementary Particle Physics

This chapter gives an overview about the fundamental particles and their interactions with each other. There will be an introduction to the particles we think are fundamental and how they could be combined to bound states. At the end of this chapter the particles and their interactions we will need later for the analysis will be introduced. More detailed information about the standard model of elementary particle physics can be found in [1].

1.1 The Standard Model of Elementary Particle Physics

1.1.1 Elementary Particles

electric charge	-1	$-\frac{2}{3}$	$-\frac{1}{3}$	0	0	$\frac{1}{3}$	$\frac{2}{3}$	1
first particle family	e^-	\bar{u}	d	$\bar{\nu}_e$	ν_e	\bar{d}	u	e^+
second particle family	μ^-	\bar{c}	s	$\bar{\nu}_\mu$	ν_μ	\bar{s}	c	μ^+
third particle family	τ^-	\bar{t}	b	$\bar{\nu}_\tau$	ν_τ	\bar{b}	t	τ^+
exchange particles of the electro-weak interaction	W^-			Z^0	γ			W^+

Table 1.1: Particles of the standard model of elementary particle physics and the exchange particles of the electro-weak interaction.

The standard model of particle physics consists of the particles we think are elementary and their interactions. The gravitation is an interaction which is important for very massive objects like planets, stars or galaxies, but isn't described within the

standard model of elementary particle physics. The interactions we will discuss now are the other three known interactions between particles – the electro-magnetic, the weak and the strong interaction. Common for all interactions is that they could only occur between particles which have a specific charge while the kind of charge, like electric charge or color charge, is different for the three interactions.

In the standard model there are three particle families everyone consisting of 2 quarks and 2 leptons. The leptons have no color charge and the neutrinos have also no electric charge while the quarks have an electric and also a color charge. An overview of the particles of the standard model is given in tab. 1.1. All interactions could be understood by the exchange of special particles typically for an interaction between the elementary particles with the specific kind of charge of the interaction.

1.1.1.1 Electro-Magnetic Interaction

The electro-magnetic interaction is known very well for a long time. It's the interaction which dominates in our daily life. It builds the atoms, binds atoms to molecules and is responsible for all chemical properties of the different elements. The electro-magnetic interaction couples on the electric charge of the particles which means that all particles which have an electric charge different from zero could have electro-magnetic interaction with each other. The interaction between two electrically charged particles could be attractive or repellent depending on the electric charge of the particles. Particles with the same sign of the charge are repellent while they are attracting to each other if the sign of the electric charge is different.

The exchange particle for this interaction is the *photon*, γ , which has no electric charge and no mass. Due to this massless exchange particle, the distance on which this interaction works between particles is unlimited but the strength is proportional to the inverse of the squared distance, $\frac{1}{r^2}$. Photons are bosons and could be real, like in the light from our sun or in the radio waves for our cell phones, but could also be virtual. Virtual particles are particles with the same properties like real particles but they could be created from the vacuum violating conservation of energy and momentum. The price for this violation is that they could be existing only for a very short amount of time.

For this interaction it's possible that particles could be created or scatter on other charged particles. In fig. 1.1 the scattering of two electrons due to this interaction is shown¹. It's impossible that a particle could decay to another particle and if a particle is created always the antiparticle of this particle is created, too. Particles could also be destroyed but only together with the same antiparticle which is the inverse process of the creation. This happens at particle collider experiments like *BABAR*. In the *BABAR* experiment electrons and positrons had been accelerated to high energies and then are brought to collision. The electrons and positrons annihilate and from the energy of both, new particles are created (fig. 1.2), which could be studied in the detector of the experiment.

Weak Interaction

The so called weak interaction is an interaction which could convert particles into others and works for all leptons and quarks. The exchange particles for this interaction are two charged bosons, W^+ and W^- , and one neutral boson, Z^0 . Scattering

¹If not stated otherwise, the time axis goes in this kind of diagrams always from left to right.

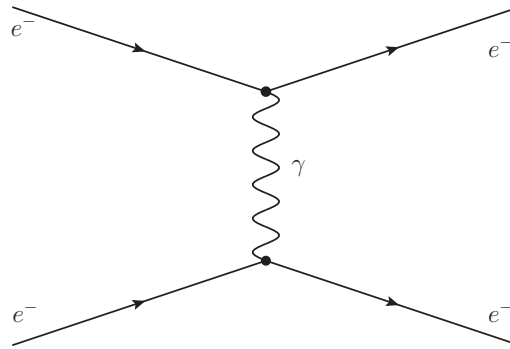
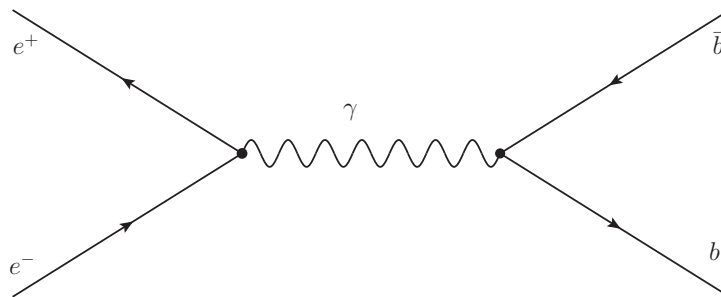


Figure 1.1: Electron-electron scattering in the electro-magnetic interaction

Figure 1.2: Electron-positron annihilation to a virtual photon and creation of a $b\bar{b}$ quark pair in the electro-magnetic interaction

of particles in this interaction is nearly the same like for the electro-magnetic interaction. The difference is that it happens via the exchange of the Z^0 instead of a γ and could also happen between electrically uncharged particles like the neutrinos. The decay of a particle happens via one of the two charged W bosons while on every interaction point (vertex) the sum of the electrical charges is conserved. The neutron decay is one example for this interaction via a W boson. In the model today, the neutron decay looks like fig. 1.3. It stands for the conversion of a d quark to an u quark via emitting a virtual W^- boson which decays then to an electron and an anti-electron-neutrino.

While the photon has no mass, the W (and Z^0) bosons have a very high mass, much higher than the mass of the d quark. But the time a virtual particle could exist is much smaller, the higher its mass. And if this exchange particle could only exist for a very short time the interaction possibility is also smaller. That's what makes the strength of this interaction so low compared to the electromagnetic-interaction and which is the origin of the name "weak interaction". That's always true for decays or reactions at energies much lower than the mass of the exchange bosons like for the neutron decay in the radioactive atoms around us, but it changes at higher energies. In experiments it was found that at energies around the mass of this bosons the strength of this interaction is no longer smaller than for the electro-magnetic interaction. Moreover, the electro-magnetic and the weak interactions merge into a combined interaction. At low energies both different interactions are only different aspects of a unified interaction. The unified interaction is called *electro-weak interaction* and is a big success of understanding and describing nature in a beautiful

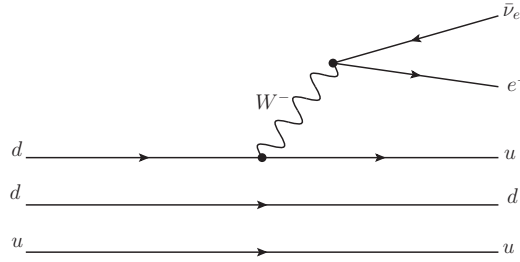


Figure 1.3: Neutron decay in the model of exchange particles.

way. The Nobel Prize in physics 1979 was awarded to Sheldon Glashow, Abdus Salam and Steven Weinberg for their work on this unified theory.

Strong Interaction

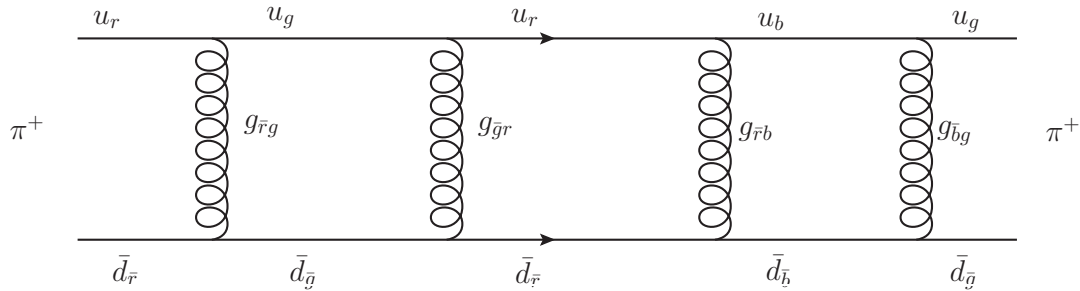
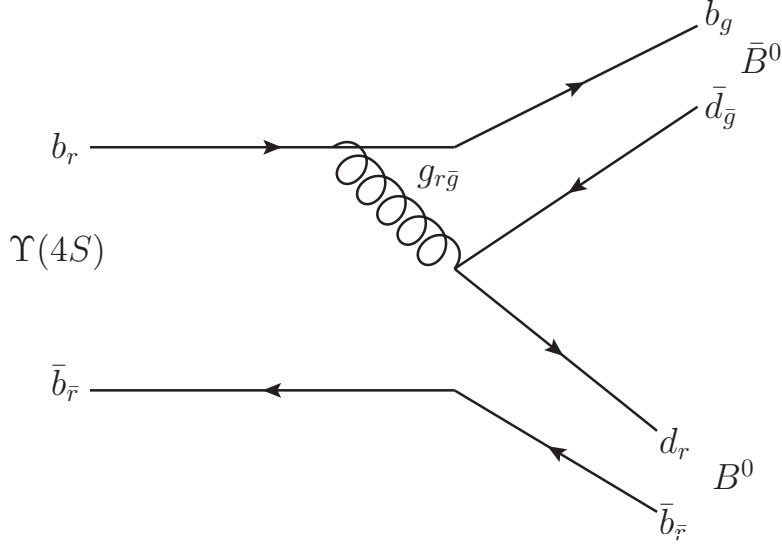


Figure 1.4: Possibilities of gluon exchange between the quarks of a pion.

The strong interaction couples on the color charge of the quarks and therefore not on leptons. This interactions binds the quarks into baryons, like protons and neutrons, and into mesons. Baryons are bound states of three quarks or anti-quarks, while mesons are bound states of a quark and an anti-quark.

This interaction works only on a very short distance between the quarks but the energy in the strong field gets higher with the distance of the quarks. This is very different to the other interactions and a reason why there couldn't exist free quarks. It's also the reason why the binding of quarks is so very strong which gave this interaction the name. The exchange particles are called *gluons*, g , which have no mass and no electric charge but carry color, too. Every gluon carries color and anticolor and the interaction of quarks happens by exchanging the color. In difference to the electric charge the color of quarks can be changed (fig. 1.4). The decay of quarks in this interaction isn't possible but the gluons could create a quark-antiquark pair which could change bound states of quarks. One example is shown in fig. 1.5 where the $\Upsilon(4S)$ meson consists of a $b\bar{b}$ pair decays to B^0 and \bar{B}^0 mesons due to the creation of a $d\bar{d}$ pair out of a gluon. The colors of the newly created quarks are the colors from the gluon. It also shows that it is impossible to create a meson out of a single gluon because such a state would not be color neutral. In this example also one possible gluon line for such a decay is shown but for all other Feynman diagrams where a $q\bar{q}$ pair is created out of gluons we will not show it anymore.

Figure 1.5: Decay of $\Upsilon(4S)$ to two neutral B mesons.

1.2 First look at the analyzed decay modes

In chapter 3 we will analyze two decay modes of the B meson, $\bar{B}^0 \rightarrow \Lambda_c^+ \bar{p} \pi^0$ and $\bar{B}^0 \rightarrow \Lambda_c^+ \bar{p} \eta$ ². In this subsection we discuss the possible decay mechanisms using Feynman diagrams and try to make a prediction for the expected ratio of branching fractions. Given that we don't have a strict theory about baryonic B -decays, we will use a phenomenological approach. There is another very similar B decay mode which has already been analyzed at *BABAR* and which we will include in our comparison of branching fraction predictions, $B^- \rightarrow \Lambda_c^+ \bar{p} \pi^-$ [2].

To get an idea which one of the different decay mechanisms are the dominant ones we have to measure the branching fraction of the decay modes and compare them with the theoretical predictions.

The quark content of the involved particles are

- $\bar{B}^0 = (b\bar{d})$
- $B^- = (b\bar{u})$
- $\Lambda_c^+ = (cud)$
- $\bar{p} = (\bar{u}\bar{d}\bar{u})$
- $\pi^- = (\bar{u}d)$
- $\pi^0 = \frac{1}{2}(d\bar{d} - u\bar{u})$
- $\eta = (\frac{1}{\sqrt{6}} \cos \theta - \frac{1}{\sqrt{3}} \sin \theta)(u\bar{u} + d\bar{d}) - (\frac{2}{\sqrt{6}} \cos \theta + \frac{1}{\sqrt{3}} \sin \theta)s\bar{s}$
- $\eta' = (\frac{1}{\sqrt{6}} \sin \theta + \frac{1}{\sqrt{3}} \cos \theta)(u\bar{u} + d\bar{d}) - (\frac{2}{\sqrt{6}} \sin \theta - \frac{1}{\sqrt{3}} \cos \theta)s\bar{s}$

²Throughout this paper charge conjugate modes are always implied.

where θ is a mixing angle. The value for θ obtained from the ratio of partial widths $\Gamma(\eta' \rightarrow \gamma\gamma)/\Gamma(\eta \rightarrow \gamma\gamma)$ is $(-18 \pm 2)^\circ$, while $\Gamma(\eta' \rightarrow \gamma\gamma)/\Gamma(\pi^0 \rightarrow \gamma\gamma)$ leads to $\sim -24^\circ$ [3].

The π^0 , η and η' are mixtures of different quarks because it doesn't matter which quarks are involved for the strong coupling between quarks – if the quarks would be massless. The quarks could change their flavor by annihilating and recreation of an $q\bar{q}$ pair. This is of course only possible for neutral electrical charged mesons. The mass of the u and d quarks are nearly the same. The mass of the s quark is approximately 20 times larger but still much lower than the mass of the c , b or t quark [3]. If in a $b\bar{b}$ bound state the quarks would annihilate and create a $d\bar{d}$ pair then the mass difference between the b and d quarks would be high enough energy that additional $q\bar{q}$ pairs from the vacuum could be created and be combined with the $d\bar{d}$. This high mass differences between the u , d , s quarks and the other quarks makes it impossible that c , b or t quarks exist in such a mixture.

1.2.1 Comparison of different decay modes

The decay mode $\bar{B}^0 \rightarrow \Lambda_c^+ \bar{p} \pi^0$ is very similar to the decay mode $B^- \rightarrow \Lambda_c^+ \bar{p} \pi^-$. For both decays there are different possibilities to combine the produced quarks to the specific final state – some are very similar for both, some are totally different. The creation of an $u\bar{u}$ or $d\bar{d}$ pair from the vacuum and the different spectator quark in the B^- (\bar{u}) and in the \bar{B}^0 (\bar{d}) is the main difference for most Feynman diagrams for both decay modes (fig. 1.6). But there are also Feynman diagrams which could contribute to only one of the decay modes. The $\bar{u}d$ from the W^- decay could create directly the π^- in the B^- decay (fig. 1.7) while for the decay of the \bar{B}^0 the W^- could interact with the \bar{d} quark from the \bar{B}^0 (fig. 1.8).

For the decay mode with the η in the final state all Feynman diagrams for the π^0 decay mode are also valid but the $u\bar{u}$ or $d\bar{d}$ don't make the π^0 state but the η . For the η decay mode there is also another Feynman diagram possible where the $q\bar{q}$ of the η is created out of gluons (fig. 1.9), but this one compared with all the other diagrams is suppressed because it is impossible to create the η out of only one gluon. It would also be possible for the decay mode with the π^0 in the final state but then it couldn't happen via gluons but only by a virtual photon which is even more suppressed. The π^0 creation out of gluons only is forbidden because the vacuum has no isospin but if a pion would be created out of gluons only, then isospin would be created. This is impossible for the strong interaction which conserves the isospin. The conservation of the isospin in the strong interaction also means that the isospin of the final state is given by the spectator quark and by the quarks coming out of the W^- , if present, in our studied decay modes.

If we assume that for two decay modes only the same Feynman diagrams are important, it would mean that the decay mechanism is the same. In this case we could use the Clebsch-Gordon-Coefficients to predict the ratio of the partial decay rates. While for the decay mode with the π^0 in the final state we have two possibilities for the isospin of the final state, $I = 1/2$ and $I = 3/2$, there is only one of them possible for the two other decay modes and it is different for the decay modes with the η ($I = 1/2$) and the π^- ($I = 3/2$) in the final state.

If we want to compare $\bar{B}^0 \rightarrow \Lambda_c^+ \bar{p} \pi^0$ with $\bar{B}^0 \rightarrow \Lambda_c^+ \bar{p} \eta$ and $B^- \rightarrow \Lambda_c^+ \bar{p} \pi^-$, we have to use different couplings in the final state and therefore different Clebsch-

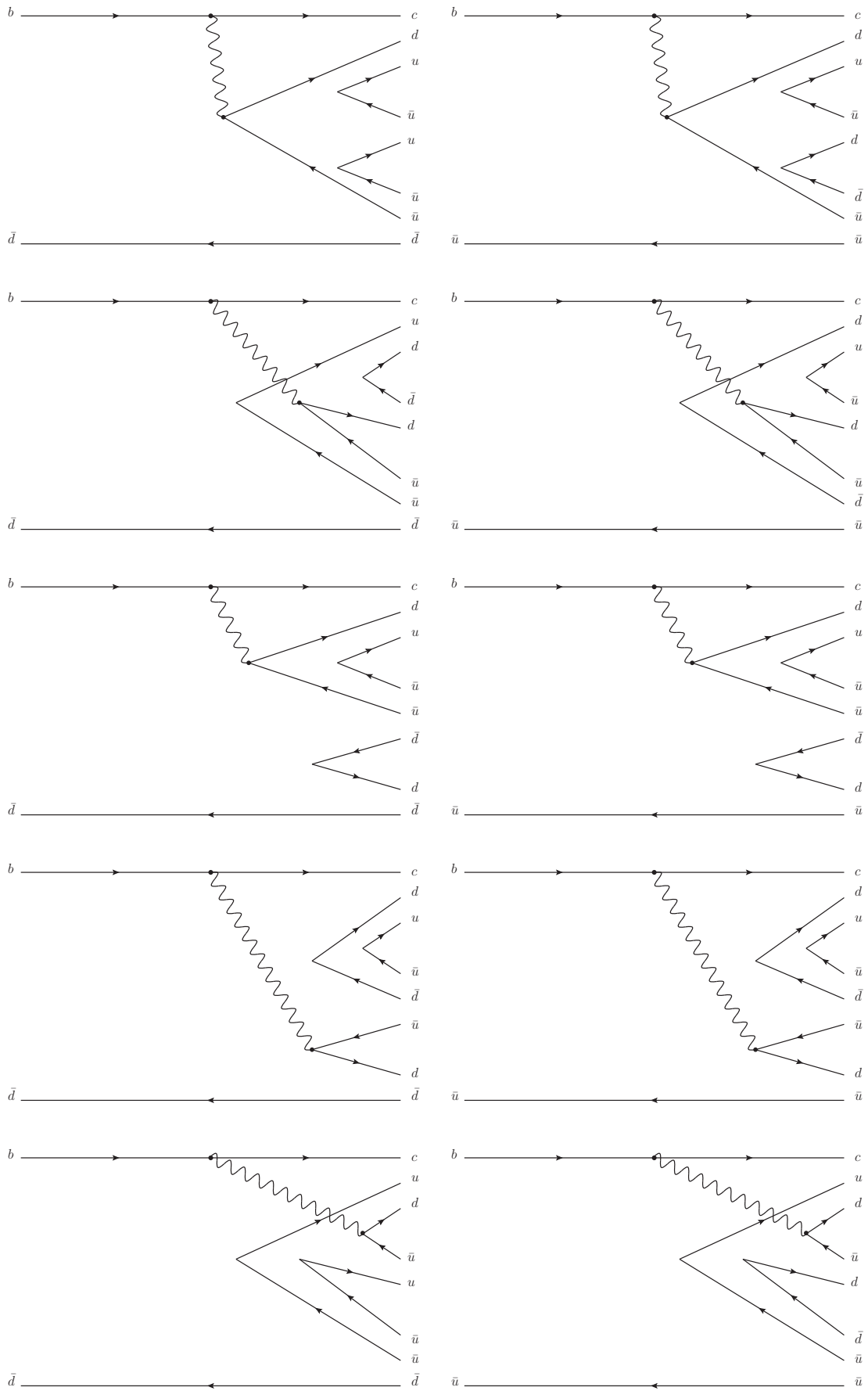


Figure 1.6: Feynman diagrams which are similar for the decay of the \bar{B}^0 (left) and the B^- (right).

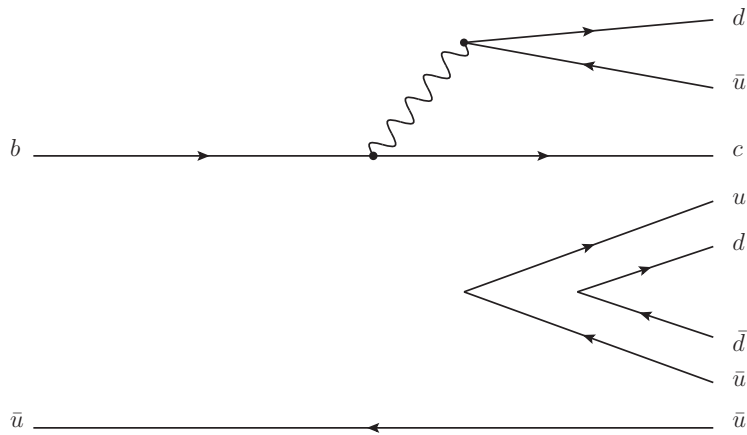


Figure 1.7: Feynman diagram where the quarks from the W^- decay are combined to a π^- which is only possible for the decay of the B^- .

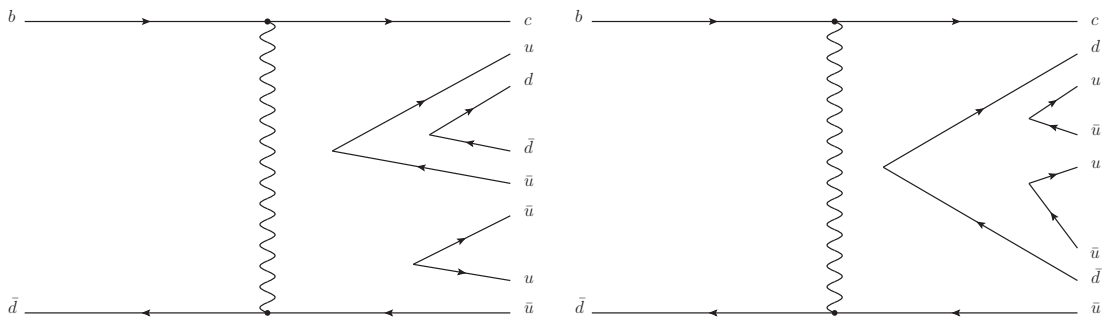


Figure 1.8: Feynman diagram where the W^- interacts with the \bar{d} from the \bar{B}^0 which is only possible for the decay of the \bar{B}^0 .

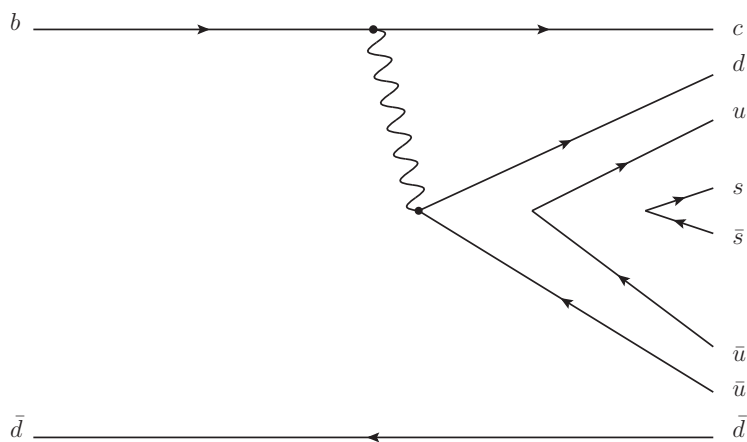


Figure 1.9: Feynman diagram where the $q\bar{q}$ ($s\bar{s}$) is created out of gluons and make the η .

Gordon-Coefficients to make sure that only final states with the same coupling of the particles are compared. But there is another final state with the same coupling like in the final state with the η and a neutral particle which is also a mixture of $u\bar{u}$, $d\bar{d}$ and $s\bar{s}$ - the η' . When we look to the possible Feynman diagrams for the \bar{B}^0 decay we find that the neutral particles in the final state are created from an $u\bar{u}$ or $d\bar{d}$ pair. Therefore, we have to calculate the probability that an $u\bar{u}$ or $d\bar{d}$ makes an η or η' and then multiply this factor with the Clebsch-Gordon-Coefficient for this coupling. We find that the probability that an η' is created out of an $u\bar{u}$ or $d\bar{d}$ is only half the probability that an η is created.

The Clebsch-Gordon-Coefficients and the resulting factor is shown in tab. 1.2. This Coefficients mean that we would expect one of the ratios in eq. (1.1) or eq. (1.2). Moreover, if the same Feynman diagrams would be the dominant ones for both compared decays than one of this equation would be fulfilled for the whole branching fraction. Using this equation we are able to find out if the weak decay of the \bar{B}^0 prefers one of the two possibilities of the isospin for the final state or not.

Table 1.2: Clebsch-Gordon-Coefficients squared for the different decays

	Clebsch-Gordon-Coeff.	final factor	isospin of the final state
$\bar{B}^0 \rightarrow \Lambda_c^+ \bar{p} \pi^0$	$\frac{1}{3}$	$\frac{1}{3}$	$I = \frac{1}{2}$
$\bar{B}^0 \rightarrow \Lambda_c^+ \bar{p} \eta$	1	$1 \cdot \frac{2}{3}$	
$\bar{B}^0 \rightarrow \Lambda_c^+ \bar{p} \pi^0$	$\frac{2}{3}$	$\frac{2}{3}$	$I = \frac{3}{2}$
$B^- \rightarrow \Lambda_c^+ \bar{p} \pi^-$	1	1	

$$\frac{\Gamma(\bar{B}^0 \rightarrow \Lambda_c^+ \bar{p} \pi^0)_{I=3/2}}{\Gamma(B^- \rightarrow \Lambda_c^+ \bar{p} \pi^-)} = \frac{2}{3} \quad (1.1)$$

$$\frac{\Gamma(\bar{B}^0 \rightarrow \Lambda_c^+ \bar{p} \pi^0)_{I=1/2}}{\Gamma(\bar{B}^0 \rightarrow \Lambda_c^+ \bar{p} \eta)} = \frac{1}{2} \quad (1.2)$$

2. The *BABAR* Experiment

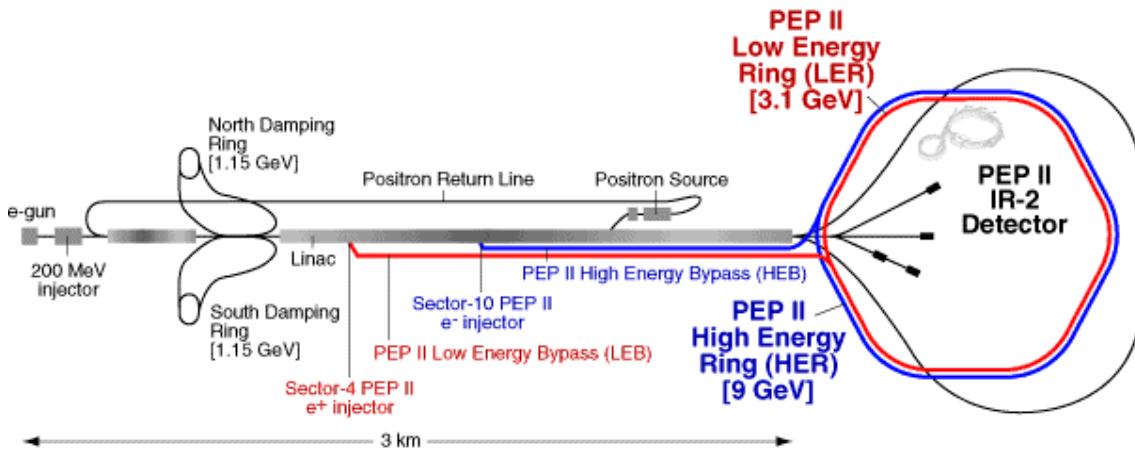


Figure 2.1: Graphics of the linear accelerator and PEP-II collider together with some basic facts, like the beam energies.

The *BABAR* detector was built at SLAC to study the CP violation in the decay of B mesons produced by the PEP-II asymmetric-energy e^+e^- collider (fig. 2.1). From 1999 to 2007, the *BABAR* experiment took data with a center-of-mass energy, \sqrt{s} , at the $\Upsilon(4S)$ resonance mass. The $\Upsilon(4S)$ decays to two B mesons (fig. 2.2). The analysis in chapter 3 are based on this data set of about 426 fb^{-1} usable data (onpeak data set) corresponding to 467 million $B\bar{B}$ pairs. An additional data sample was taken 40 MeV below the mass of the $\Upsilon(4S)$ resonance (offpeak data set) which we use to study the continuum background $e^+e^- \rightarrow q\bar{q}$, where $q = u, d, s$ or c . Details about the used data luminosity can be found in Table 2.1.

The *BABAR* collaboration consist of several hundred physicist from about 10 countries. This makes it necessary that the analyses framework and data analyses tools are using a common standard and tools are prepared for doing analyses efficiently. In the next sections the *BABAR* detector and the basics of the analysis framework will be described. All pictures in this section are taken from the official *BABAR* detector information system [4]. The coordinate system is defined in a way that the z -axis goes along the e^+e^- beam direction.

Table 2.1: Usable data luminosity and number of $B\bar{B}$ pairs of the different time periods.

	onpeak Luminosity (fb^{-1})	$N(B\bar{B})$ (10^6)	offpeak Luminosity (fb^{-1})
Run 1	19.9	$21.89 \pm 0.02 \pm 0.24$	2.6
Run 2	61.1	$67.39 \pm 0.04 \pm 0.74$	6.9
Run 3	32.3	$35.57 \pm 0.03 \pm 0.39$	2.5
Run 4	100.3	$110.45 \pm 0.06 \pm 1.21$	10.1
Run 5	133.3	$147.19 \pm 0.06 \pm 1.62$	14.5
Run 6	78.8	$84.77 \pm 0.05 \pm 0.93$	7.9
Run 1-6	425.5	$467.26 \pm 0.11 \pm 5.14$	44.5

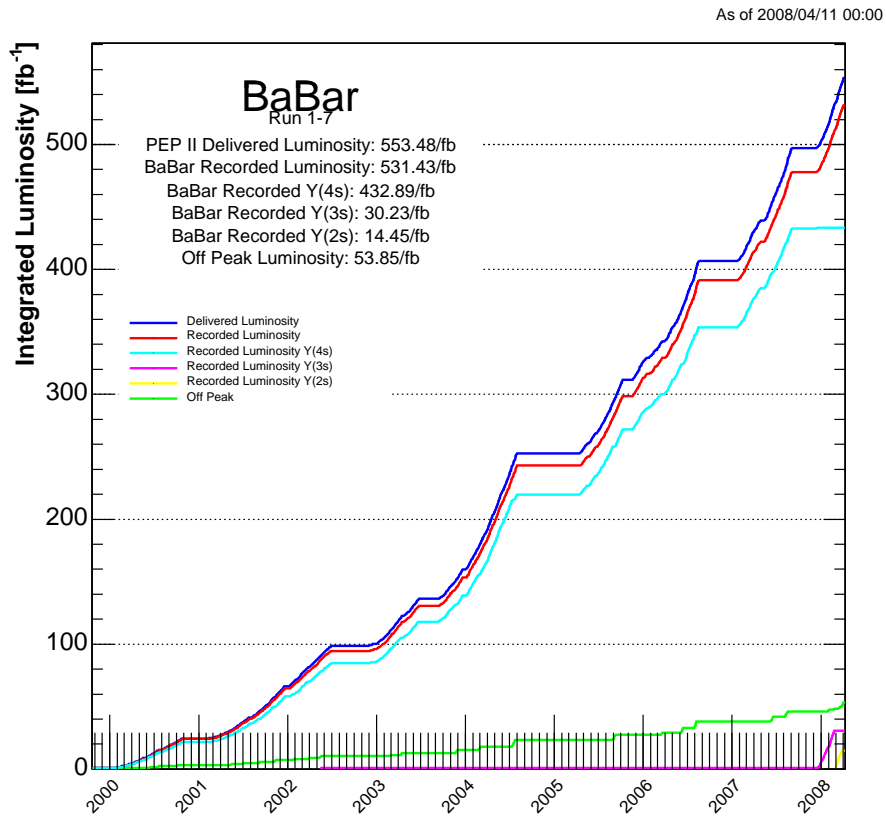


Figure 2.2: Recorded luminosity during the lifetime of the *BABAR* experiment.

2.1 The *BABAR* detector

The *BABAR* detector (fig. 2.3) was built at the interaction region of the electron-positron beams and consists of different parts, each built for a specific task in particle detection and identification. The different parts of the detector are:

- Vertex Detector
- Tracking Chamber
- Cherenkov Detector
- Electron and Photon Detector
- Magnet Coil
- Muon and Hadron Detector

Within the detector exists a magnetic field to be able to measure the electric charge of the particles and their momentum. Every electrical charged particle change the direction of movement within a magnetic field. The sign of the electric charge of the particle gives the direction in which the track of this particle curves and the momentum can be determined from the curvature of the track. Detailed information about the detector can be found in [5].

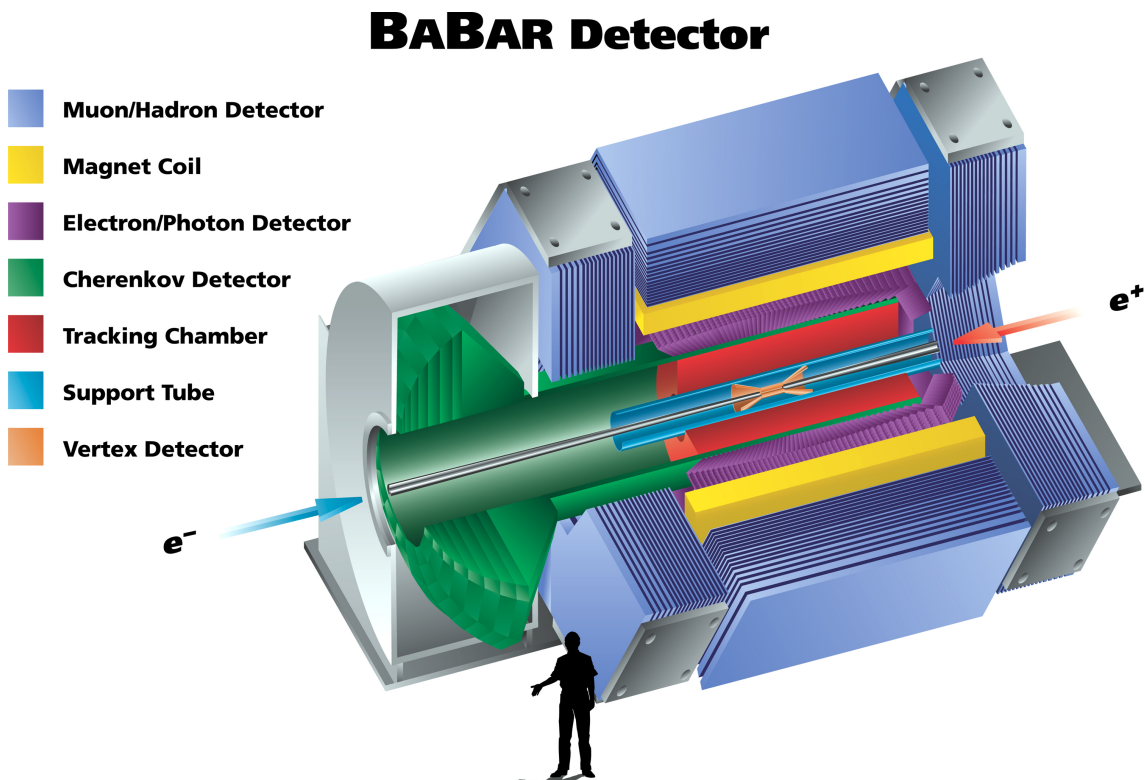


Figure 2.3: Schematic view of the constituent parts of the *BABAR* detector.

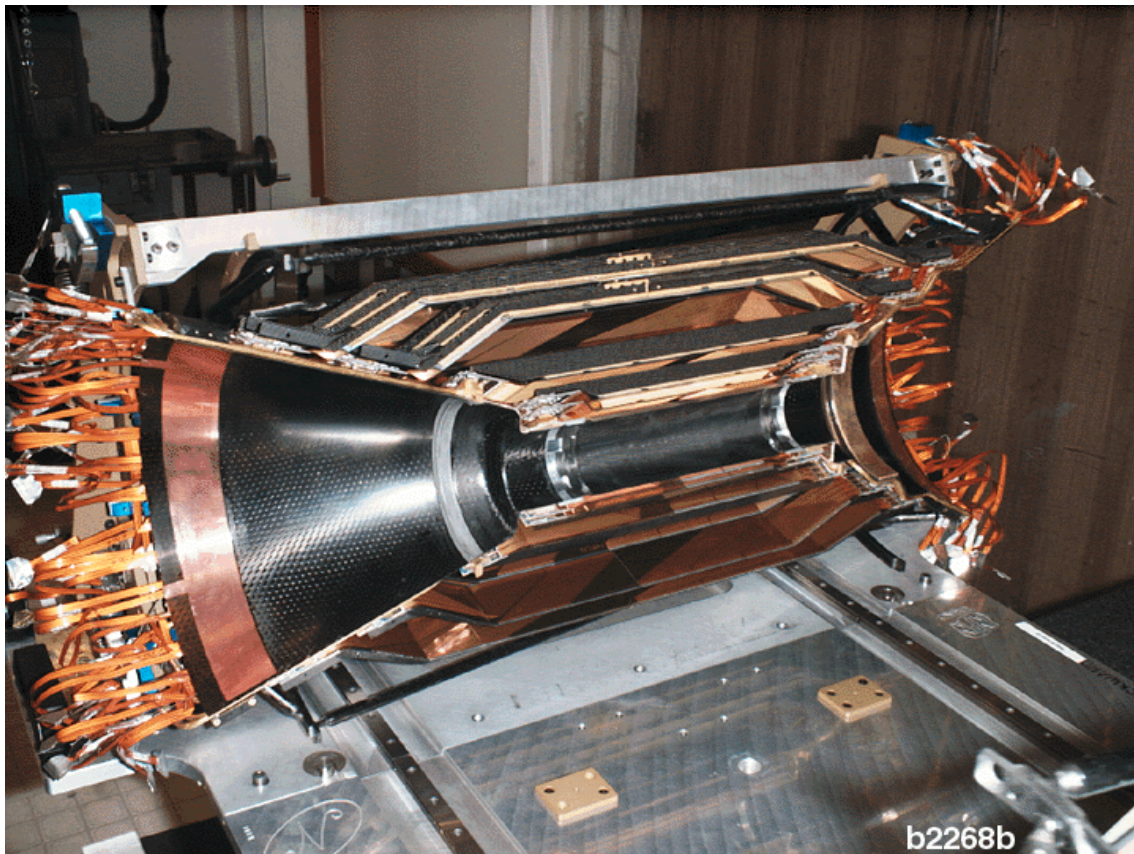


Figure 2.4: One half of the SVT seen from the inside direction.

2.1.1 Silicon Vertex Detector (SVT)

The Vertex detector (fig. 2.4) is used to measure particle tracks very close to the interaction point. To ensure that these tracks are measured before any other interactions with material happen, this detector device is located within the supporting tube. The supporting tube is a structure which supports the beam pipe. That is why the SVT is the only tracking device used to measure very low momentum electrical charged particles which do not reach the other parts of the detector.

The SVT consists of five concentric polyhedral layers of double-sided silicon microstrip detectors which are divided in many small parts to ensure a good resolution in measuring the track position. The whole SVT has about 150000 read out channels. For particle identification the energy loss, dE/dx , is measured.

2.1.2 Tracking Chamber (DCH)

The tracking chamber (fig. 2.5) is a gas-filled drift chamber which contains different kinds of wires. The gas is a helium based mixture and the DCH consists of 40 concentric cylindrical layers of wires. Each of these layers is made of 7104 drift cells.

In the DCH there are field wires to provide an electrical field. If an electrical charged particle goes through the DCH it ionizes the gas in it and the resulting electrons drift in the electric field. To detect these electrons there are sense wires in the drift chamber. From the time it takes for the electrons to reach the next sense wire the position of the particle track could be determined. The main task for the DCH

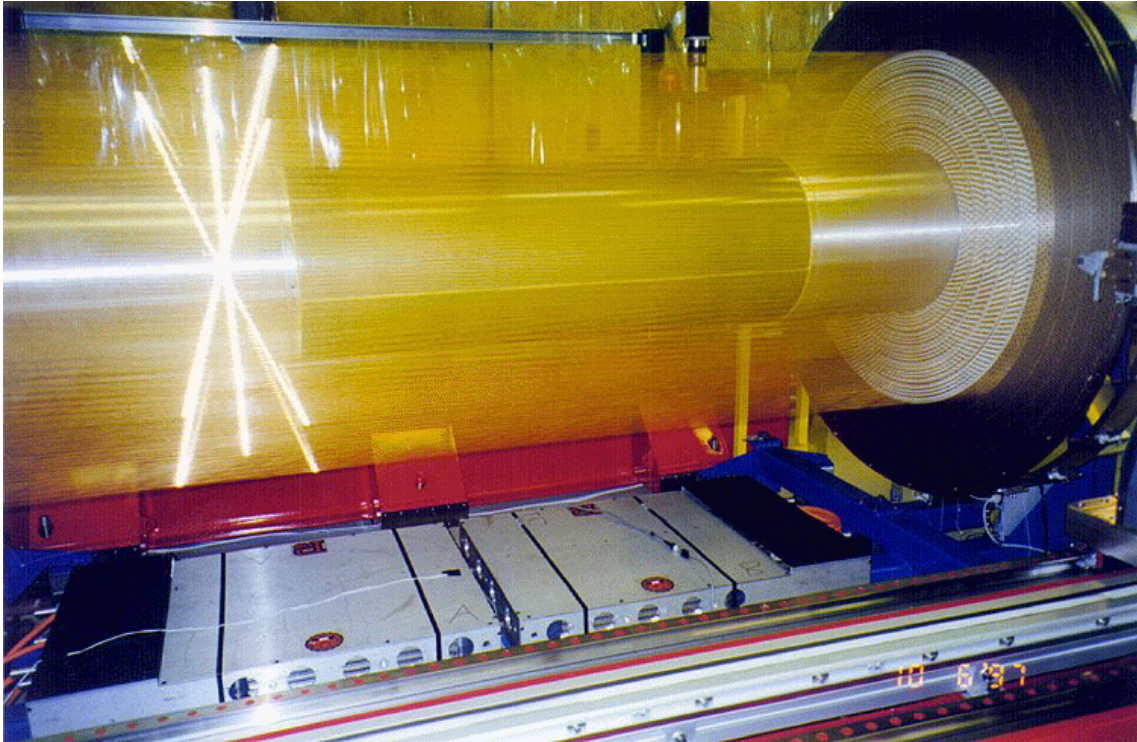


Figure 2.5: The DCH with all wires in it.

is to obtain a very good momentum resolution for electrical charged tracks. This can be done because the DCH is in a magnetic field and the charged particles curve. From the curvature the momentum is determined. The DCH is also used for particle identification using the information about the energy loss, dE/dx .

2.1.3 Cherenkov Detector (DIRC)

DIRC stands for “Detector of Internal Reflected Cherenkov light” and is a device for particle identification. While it is impossible for a particle to have a velocity faster than the velocity of light in vacuum (c), the velocity in matter could be higher than for light in this matter. Whenever a electrical charged particle has a velocity in matter higher than for light in this medium, radiation is emitted, called Cherenkov light. This radiation is emitted under a constant angle in respect to the flight direction of the particle. The angle depends only on the velocity of the particle. Together with momentum measurement in the SVT and DCH, the mass of the particle can be calculated.

The DIRC consists of 144 quartz bars which are arranged in a twelve-sided polygon around the beam line. Electrical charged particles going through this quartz bars could generate Cerenkov radiation in it. The photons are transferred by total internal reflection to a large water tank. The angle is preserved in this process. At the outside of the water tank there are about 11000 photomultiplier tubes to detect the photons (fig. 2.6). The Cerenkov angle is determined from the photon position and the original track position.

2.1.4 Electron and Photon Detector (EMC)

The device for electron and photon detection is the electro-magnetic Calorimeter and measures the energy of these particles. Electrons and photons are absorbed in

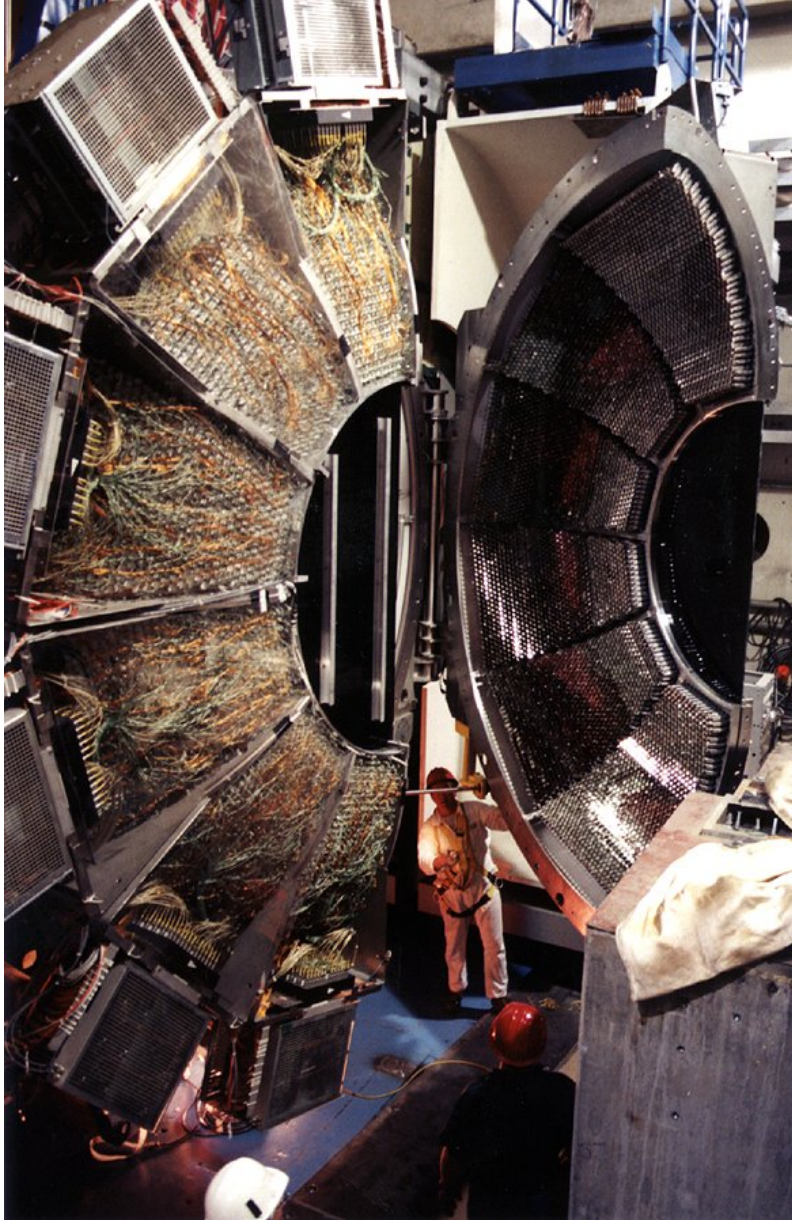


Figure 2.6: View of the photomultiplier tubes installed in the DIRC.

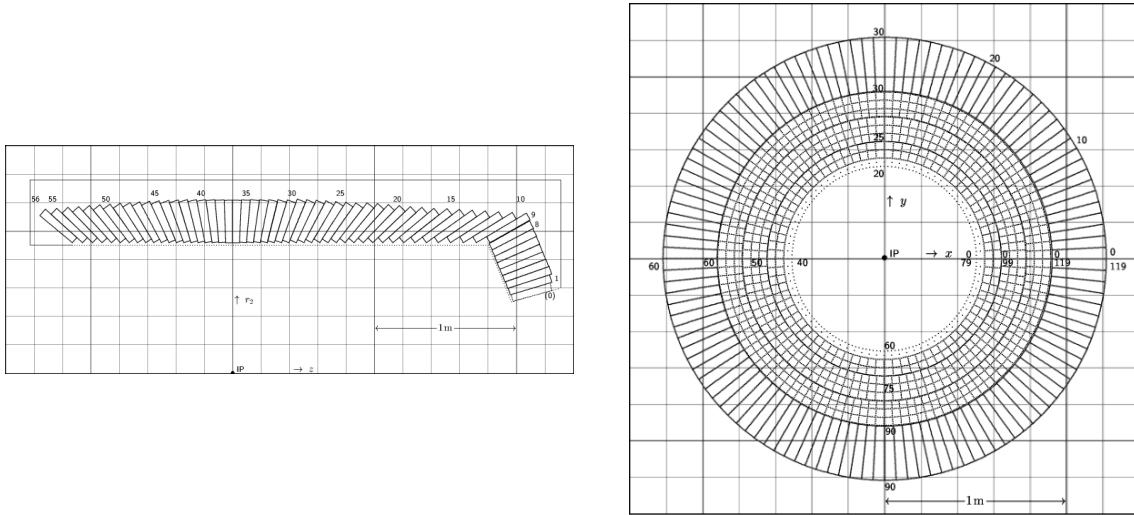


Figure 2.7: Schematic view how the crystals of the EMC are arranged in the r - z -plane (left) and x - y -plane (right).

the EMC and therefore the energy of this particles is deposited in the EMC and can be measured.

The EMC consists of about 6000 CsI(Tl) crystals. Fig. 2.7 shows how they are arranged around the beam pipe. Due to so many crystals installed, it is also possible to determine the position of the particle in the EMC. This is for neutral particles the only information to assume a flight direction. The information of the lateral shower shape of the electromagnetic radiation in the EMC (LAT) and in how many crystals this radiation associated with one particle is detected, is also used for PID. The LAT parameter describes the lateral energy distribution in the EMC and is defined as

$$LAT = \frac{\sum_{i=3}^N E_i r_i^2}{\sum_{i=3}^N E_i r_i^2 + E_1 r_0^2 + E_2 r_0^2} \quad (2.1)$$

were N is the number of crystals associated to the shower, E_i the energy deposited in the i -th crystal, r_i the lateral distance between the center of the shower and the i -th crystal, and $r_0 = 5\text{cm}$ which is the average distance between two crystals. It is also defined that $E_1 > E_2 > \dots > E_N$.

2.1.5 Magnet Coil

A magnet field is needed to measure the momentum of charged particles and the sign of the electrical charge. To provide this magnetic field a superconducting solenoid is located between the EMC and the Muon Detector. The magnetic field is set to $1.5T$.

2.1.6 Muon and Hadron Detector

The flux return at *BABAR* is made of layers of iron and steel. Between these layers are detectors to detect penetrating particles, like muons, and neutral particles, like K^0 . That's why this detector element is called IFR, Instrumented Flux Return.

2.2 BABAR Framework

The *BABAR* software *Beta* is written in C and C++, and organized in many different packages, e.g. packages which provide particle identification. To reconstruct a specific *B* decay mode, like $\bar{B}^0 \rightarrow \Lambda_c^+ \bar{p} \pi^0$ and $\Lambda_c^+ \rightarrow p K^- \pi^+$, we have to reconstruct the tracks of the particles and to identify charged particles as protons, kaons or pions. This is automatically done in the framework every time an event is loaded. Next in reconstruction we have to get the energy and momentum information of a track which is also provided by the framework using the measured detector information for this track. This section describes how the particle selection, used for the analysis, within the *BABAR* frameworks works.

2.2.1 Trigger System and Track Reconstruction

There are two triggers at *BABAR*, the L1 and L3 trigger, for preselecting interesting physics events and to suppress background events, like $e^+e^- \rightarrow e^+e^-$. While L1 is realized in hardware at the different detector elements, L3 is a software trigger running on a linux computing farm after the event information from the single detector elements have been collected. The total trigger rate for L1 was about 2500Hz. The L3 software trigger analyzed the information from the DCH and EMC and makes an online event reconstruction at a rate of about 100Hz. The determination of the luminosity based on $e^+e^- \rightarrow \mu^+\mu^-$ is also done by the L3 system. The output of the L3 system is used for track reconstruction and then for physics analyses.

For the reconstruction of charged tracks a Kalman filter based on the SVT and DCH information is used [5]. The information of both systems are analyzed independently and merged together to a single track. This track is extrapolated to the EMC and IFR. The information from these two detector elements are stored together with the tracking and DIRC information for a single charged particle candidate. All found tracks from a single event are stored together in a global tracking list which is used as the input for particle identification and user analyses.

2.2.2 Charged Particle Identification using Likelihood Selectors

For the identification of charged particles the vertex tracker, Cherenkov detector and tracking chamber are used. To reconstruct photons and π^0 only the EMC information is used. Clusters of deposited energy in EMC which do not match to any charged track are used as photon candidates.

For the different detector elements a Likelihood is calculated which is a measure how good the current track matches a given particle hypothesis. These Likelihoods will be calculated for the hypotheses that a charged track is a proton, kaon or pion. The Likelihoods for all detector elements will be multiplied to give the overall Likelihood.

The energy loss of an electrical charged particle going through the SVT and DCH are used for identification of this particle. The energy loss happens by ionizing the absorber and is given by the *Bethe-Bloch* formula

$$-\frac{dE}{dx} = \text{const.} \cdot \frac{Z}{A} \cdot \frac{q^2}{\beta^2} \left(\frac{1}{2} \ln \left(\frac{2m_e c^2 \beta^2 E_{kin}(\text{max})}{I^2 (1 - \beta^2)} \right) - \beta^2 \right). \quad (2.2)$$

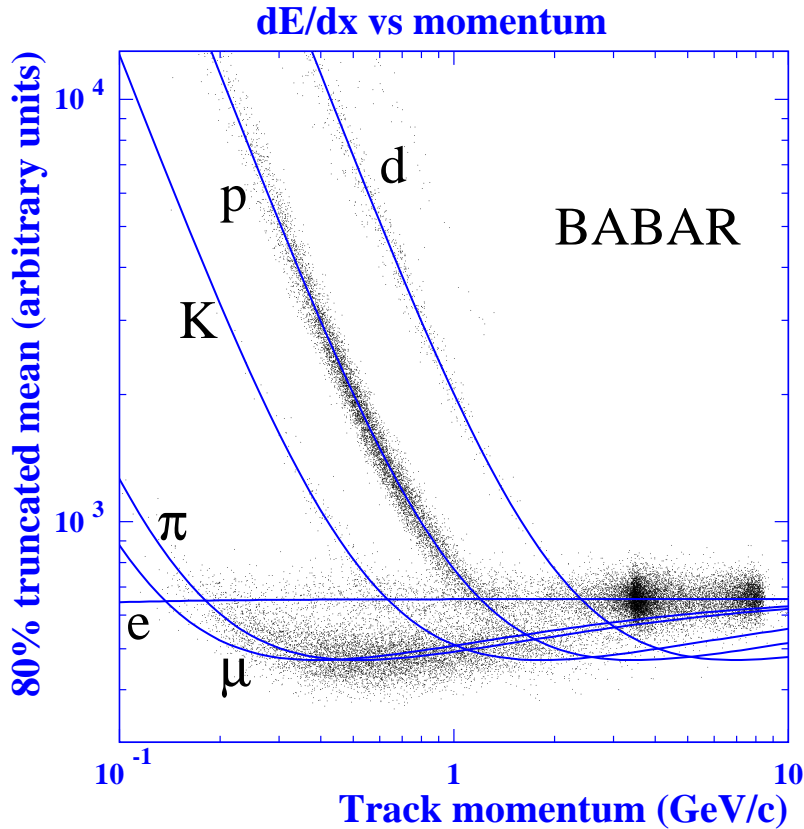


Figure 2.8: Energy loss as a function of the momentum $p = mv$

where the different variables are defined in tab. 2.2.

The Bethe-Bloch formula means that the ionization of the passing particle depends only on the velocity and electric charge of this particle while everything else is constant for a specific absorber.

The energy loss in the DCH for different particles is shown in fig. 2.8. Using this information, the Likelihood for a given particle hypothesis is computed by

$$\mathcal{L} \sim e^{-\frac{\left(\frac{dE}{dx}(\text{meas.}) - \frac{dE}{dx}(\text{expect.})\right)^2}{\left(\Delta\frac{dE}{dx}\right)^2}} \quad (2.3)$$

where $dE/dx(\text{meas.})$ is the measured value for the energy loss in the experiment, $dE/dx(\text{expect.})$ the expected value for different particle hypothesis using the measured momentum, and $\Delta(dE/dx)$ the uncertainty on dE/dx .

For electrical charged particles going through matter with a velocity higher than the one of light in this matter, photons are emitted in an angle ϑ around the flight direction. This angle is given by

$$\vartheta = \arccos\left(\frac{1}{n\beta}\right) \quad (2.4)$$

where $n = 1.473$ is the refractive index of the quartz bars used in the DIRC and β again the velocity in units of c . For the DIRC Likelihood the expected angle of the

Variable	Definition
Z	number of nucleus of the absorber
A	mass of the nucleus of the absorber
m_e	electron mass
c	speed of light in vacuum
q	electric charge of the particle going through the absorber
β	velocity of the passing particle (in units of c)
$E_{\text{kin}}(\text{max})$	highest kinetic energy which a free electron could have after a collision
I	mean excitation energy of the absorber atoms

Table 2.2: Definition of the variables in the Bethe-Bloch-Formula

emitted photons in respect to the flight direction is compared with the measured angle. This results in a DIRC Likelihood of

$$\mathcal{L} \sim e^{-\frac{(\vartheta_{\text{meas.}} - \vartheta_{\text{expect.}})^2}{(\Delta\vartheta)^2}} \quad (2.5)$$

where the indices have the same meaning as for the DCH Likelihood.

The overall Likelihood is given by

$$\mathcal{L} = \mathcal{L}_{\text{SVT}} \times \mathcal{L}_{\text{DCH}} \times \mathcal{L}_{\text{DIRC}}. \quad (2.6)$$

and computed for all particle hypothesis resulting in \mathcal{L}_p , \mathcal{L}_K and \mathcal{L}_π . To decide if a particle could be a specific one, Likelihood ratios like $\mathcal{L}_K/(\mathcal{L}_K + \mathcal{L}_p)$ or $\mathcal{L}_p/(\mathcal{L}_p + \mathcal{L}_\pi)$, are computed. Selection criteria on this ratios are used to make a decision whether a particle is used for a specific particle hypothesis or not.

3. Decay reconstruction

3.1 Event characteristics for B reconstruction at *BABAR*

The center-of-mass energy of the experiment is adjusted to the mass of the $\Upsilon(4S)$. The $\Upsilon(4S)$ is a $b\bar{b}$ bound state with an invariant mass $m(\Upsilon(4S)) \approx 2 \cdot m(B)$ and therefore can decay to two B mesons. This decay is a process of the strong interaction as shown in fig. 1.5. The created B mesons have only a very small momentum in the $\Upsilon(4S)$ rest frame due to the small mass differences and the decay vertexes of this mesons couldn't be separated because they would be nearly at the same position. Therefore, the beam energies are asymmetric which gives the $\Upsilon(4S)$ a non-zero momentum in the laboratory frame. This is conserved in the decay of the $\Upsilon(4S)$. Due to this momentum conservation the B mesons have also a momentum in the laboratory frame which is different to the $\Upsilon(4S)$ rest frame, due to the asymmetric beam energies. The energy of the e^- beam is about 9.0 GeV and 3.1 GeV for the e^+ beam.

For the analyses of B decays two variables are used at *BABAR*. These variables are ΔE and m_{ES} which make use of the special event characteristic. In the center-of-mass frame the energy of the B mesons, $E^*(B)$, is half the energy of the $\Upsilon(4S)$, $E^*(B) = 1/2\sqrt{s}$. ΔE is defined as $\Delta E = E^*(B) - 1/2\sqrt{s}$ which is zero for correctly reconstructed B candidates. The invariant mass of a particle is defined as $m = \sqrt{E^*(B)^2 - p^*(B)^2}$, where $p^*(B)$ is the momentum of the B candidate in the center-of-mass frame. Using the information of ΔE we could substitute the energy of the B candidate in the definition of the invariant mass with $1/2\sqrt{s}$ which leads to $m_{\text{ES}} = \sqrt{(1/2\sqrt{s})^2 - p^*(B)^2}$. If the center-of-mass frame would be the same like the laboratory frame then both variables would be independent. But due to the asymmetric beam energies we need to transform the measured quantities from the laboratory frame to the center-of-mass frame which makes them no longer independent from each other. To make them independent again we have to use only quantities from the laboratory frame which leads to

$$\Delta E = E^*(B) - \frac{1}{2}\sqrt{s} \quad (3.1)$$

and

$$m_{\text{ES}} = \sqrt{\left(\frac{s + 2\mathbf{p}_0\mathbf{p}_B}{2E_0}\right)^2 - \mathbf{p}_B^2}. \quad (3.2)$$

and is the same equation for ΔE like before.

3.2 Simulated Events

To determine the reconstruction efficiency and to look for possible peaking background sources, a detailed GEANT4 Monte Carlo (MC) simulation of the *BABAR* detector is used. It generates MC events uniformly in the phase space of the simulated decay mode. Peaking background would show up in the fitted distribution like signal and therefore must be removed or at least the fraction must be known. *B*-decay modes for which MC events are used are listed in table 3.1 and inclusive samples of simulated events for general background studies are listed in table 3.2. Simulated events are also used to determine selection criteria.

Table 3.1: Simulated *B* decay modes used in the analysis.

\bar{B}^0/B^- - decay mode	number of generated events
$\Lambda_c^+ \bar{p} \pi^0$	387000
$\Sigma_c^+(2455) \bar{p}$	195000
$\Sigma_c^+(2520) \bar{p}$	195000
$\Sigma_c^+(2800) \bar{p}$	195000
$\Lambda_c^+ \bar{p} \eta$	725000
$\Lambda_c^+ \bar{p} \pi^-$	1890000
$\Sigma_c^0(2455) \bar{p}$	387000
$\Sigma_c^0(2520) \bar{p}$	387000
$\Sigma_c^0(2800) \bar{p}$	387000
$\Lambda_c^+ \bar{p}$	392000
$\Lambda_c^+ \bar{p} \pi^- \pi^0$	392000
$\Lambda_c^+ \bar{p} \pi^+ \pi^-$	4987000
$\Sigma_c^0(2455) \bar{p} \pi^+$	271000
$\Sigma_c^0(2520) \bar{p} \pi^+$	269000
$\Sigma_c^0(2800) \bar{p} \pi^+$	271000
$\Sigma_c^{++}(2455) \bar{p} \pi^-$	271000
$\Sigma_c^{++}(2520) \bar{p} \pi^-$	271000
$\Sigma_c^{++}(2800) \bar{p} \pi^-$	271000
$\Lambda_c^+ \bar{p} \pi^+ \pi^- \pi^-$	271000
$\Lambda_c^+ \bar{p} \pi^+ \pi^- \pi^0$	271000

3.3 Reconstruction of $\bar{B}^0 \rightarrow \Lambda_c^+ \bar{p} \pi^0$

For the reconstruction of this decay mode we only use the decay channels $\Lambda_c^+ \rightarrow p K^- \pi^+$ and $\pi^0 \rightarrow \gamma \gamma$. While the branching fraction for the π^0 decay is known very

Table 3.2: Simulated inclusive MC modes used for background studies in the analysis.

simulated mode	number of generated events
$e^+e^- \rightarrow B^0\bar{B}^0$	735.850×10^6
$e^+e^- \rightarrow B^+B^-$	731.146×10^6
$e^+e^- \rightarrow u\bar{u}, d\bar{d}$ and $s\bar{s}$	860.570×10^6
$e^+e^- \rightarrow c\bar{c}$	1036.084×10^6

well to be $(98.823 \pm 0.034)\%$, the branching fraction $\mathcal{B}(\Lambda_c^+ \rightarrow pK^-\pi^+) = (5.0 \pm 1.3)\%$ has a very large uncertainty [3]. To take this external uncertainty into account it will not be included in the systematic uncertainty of any result but quoted separate. This makes it possible to reduce the overall uncertainty once the branching fraction of the Λ_c^+ will be known better. The current analysis and the results are already published in [6]. The CLEO collaboration previously set an upper limit of $\mathcal{B}(\bar{B}^0 \rightarrow \Lambda_c^+ \bar{p} \pi^0) < 5.9 \times 10^{-4}$ [7].

For the reconstruction of the Λ_c^+ we combine p , K^- and π^+ candidates and use a fit with a geometric constraint applied to the common vertex of these daughter particles. To form a \bar{B}^0 candidate we combine the Λ_c^+ and π^0 candidates with a \bar{p} candidate in a fit to a common vertex and using additional kinematic constraints. In this fit the mass of the $pK^-\pi^+$ candidate is constrained to the mass of the Λ_c^+ and the mass of the $\gamma\gamma$ combination to the mass of the π^0 .

To show that this decay mode exists we have to prove that the reconstruction of the daughter particles of the \bar{B}^0 , Λ_c^+ and π^0 , is working. It must also be shown that there is no so called ‘‘peaking background’’ which would increase the number of signal events. To raise the significance of the signal, $S^2/(S+B)$ is maximized, where S is the number of signal events and B the number of background events. We obtain both numbers from MC simulations or data as described below.

Within the *BABAR* framework there are already some predefined lists of charged (tracking list) and neutral (neutral list) candidates and also for the different kind of particles (PID lists). All of these lists have different properties depending on the wanted purity or efficiency of a specific kind of particle. We optimize the selection of the tracking lists, PID lists and all the selections on the properties of the Λ_c^+ on data using the comparable and already known decay mode $B^- \rightarrow \Lambda_c^+ \bar{p} \pi^-$. To determine the number of signal and background events the ΔE distribution for the decay mode $B^- \rightarrow \Lambda_c^+ \bar{p} \pi^-$ with the different selections applied is fitted in the range $-0.1 < \Delta E < 0.1$ GeV. In the fit only the background is fitted by a first order polynomial assuming the background is smooth under the signal and outside of it. The number of background events is directly given by the fit while the difference between the ΔE distribution and the fit is used for the number of signal events in the optimization process. Properties other than described before are optimized using simulated events. The number of signal events after a selection is given by simulated events of the studied signal mode, while the number of background events is determined from the MC modes listed in tab. 3.2 where the signal mode is removed from $e^+e^- \rightarrow B^0\bar{B}^0$.

3.3.1 Selection criteria

The following criteria are the result of the whole optimization process and will be used for the reconstruction of the B -decay:

- charged tracks must origin within 1.5 cm of the beam spot in the xy-plane and within 2.5 cm in the z-direction
- no PID list used for π^- identification; all charged tracks are used as pion candidates
- PID lists using Likelihood selectors for particle identification with the following criteria are used :
 - protons from Λ_c^+ must fullfil: $\frac{\mathcal{L}_p}{\mathcal{L}_K + \mathcal{L}_p} > 0.7000$, $\frac{\mathcal{L}_p}{\mathcal{L}_p + \mathcal{L}_\pi} > 0.5000$ and must not be in a predefined electron list if they have momentum higher than 0.7 GeV/c
 - kaons from Λ_c^+ must fullfil: $\frac{\mathcal{L}_K}{\mathcal{L}_K + \mathcal{L}_\pi} > 0.8176$, $\frac{\mathcal{L}_K}{\mathcal{L}_p + \mathcal{L}_K} > 0.0180$ and must also not be in a predefined electron list if they have a momentum higher than 0.4 GeV/c
 - protons from the \bar{B}^0 must fullfil: $\frac{\mathcal{L}_p}{\mathcal{L}_K + \mathcal{L}_p} > 0.2500$, $\frac{\mathcal{L}_p}{\mathcal{L}_p + \mathcal{L}_\pi} > 0.5000$
- $2.276 \text{ GeV}/c^2 < m(pK^-\pi^+) < 2.296 \text{ GeV}/c^2$ (within 2.5σ of the fitted peak of the mass distribution for the Λ_c^+ candidate)
- Probability for $(p K^- \pi^+)$ vertex fit > 0.001
- $E(\gamma_1) > 0.06 \text{ GeV}$
- $E(\gamma_2) > 0.10 \text{ GeV}$ (it's always: $E(\gamma_1) < E(\gamma_2)$)
- $0.06 < \text{lat}(\gamma_1) < 0.80$
- $0.10 < \text{lat}(\gamma_2) < 0.80$
- $0.120 \text{ GeV}/c^2 < m(\gamma\gamma) < 0.145 \text{ GeV}/c^2$ for the π^0 candidate
- Probability for B_{cand} fit > 0.001 (fit to a common vertex and using mass constraints for π^0 and Λ_c^+ candidates)

The efficiency for the kaon selection is around 90% while the rate for misidentifying pions and protons as kaons varies between 5% and 10%, depending on track momentum. The identification efficiency for the proton selection is greater than 90% while the misidentification rate of identifying kaons and pions as protons varies between 3% and 15%, depending on track momentum.

In addition to the previous criteria there is also a selection of only one signal candidate per event. In events with more than one candidate (about 10% of the events), first the candidate(s) with the invariant mass $m(\gamma\gamma)$ closest to the π^0 nominal mass are selected. For events with multiple candidates containing the same π^0 , the candidate(s) with the invariant mass $m(pK^-\pi^+)$ closest to the Λ_c^+ nominal mass are

retained. If there are still multiple B candidates, the one with the highest probability of the kinematic and vertex fit is used.

Furthermore, other B decays with more or less particles in the final state show up as signal in the m_{ES} variable, too. But this events are shifted in ΔE to lower or higher values. That's why we use only signal candidates around $\Delta E = 0 \text{ GeV}$ for the reconstruction of the studied decay mode. The best relation between signal and background events to maximize the significance is for $-0.05 < \Delta E < 0.04 \text{ GeV}$.

3.3.2 Peaking background

Peaking background could come from a B -decay mode which is very similar to the studied signal mode. In this case also after all selection criteria there would be still a signal peak not coming from the signal mode which would enhance the number of signal candidates. To avoid this, we study generic MC events and also MC events for some specific B decay modes which could contribute to the signal. A list of this decay modes can be found in Tab.3.1.

In this study we find that the mode $B^- \rightarrow \Lambda_c^+ \bar{p} \pi^-$ and its subchannels $B^- \rightarrow \bar{p} \Sigma_c^0(2455, 2520, 2800)$ are a source for peaking background. The m_{ES} distributions with the cuts described in sec. 3.3.1 show a large enhancement around $5.28 \text{ GeV}/c^2$ (fig.3.1, black data points). The 2-dimensional plots for m_{ES} and ΔE are shown in fig.3.2.

To get rid of this background we also reconstruct the mode $B^- \rightarrow \Lambda_c^+ \bar{p} \pi^-$ in every event. For this reconstruction the same selection criteria on the Λ_c^+ candidate, tracking and PID lists are used. For the additional charged pion candidate charged tracks are used without any PID criteria. We will not use the whole event for the signal reconstruction if the mass of the $\Lambda_c^+ \pi^-$ -system is between $2.400 \text{ GeV}/c^2$ and $2.465 \text{ GeV}/c^2$, or if m_{ES} for this mode is greater than $5.27 \text{ GeV}/c^2$ and ΔE is between -0.05 GeV and 0.05 GeV (veto cuts). This removes nearly all of this kind of background while the remaining background doesn't peak anymore. The m_{ES} distributions after these veto cuts are shown as the red data points in fig.3.1. With this veto cuts these distributions are well described by an ARGUS function (eq.3.3, [8]) which is usually used to describe the combinatorial background in m_{ES} .

$$f_{\text{ARGUS}} = n \cdot m_{\text{ES}} \sqrt{1 - \left(\frac{m_{\text{ES}}}{m_{\text{end}}}\right)^2} \cdot e^{-c \left(1 - \left(\frac{m_{\text{ES}}}{m_{\text{end}}}\right)^2\right)} \quad (3.3)$$

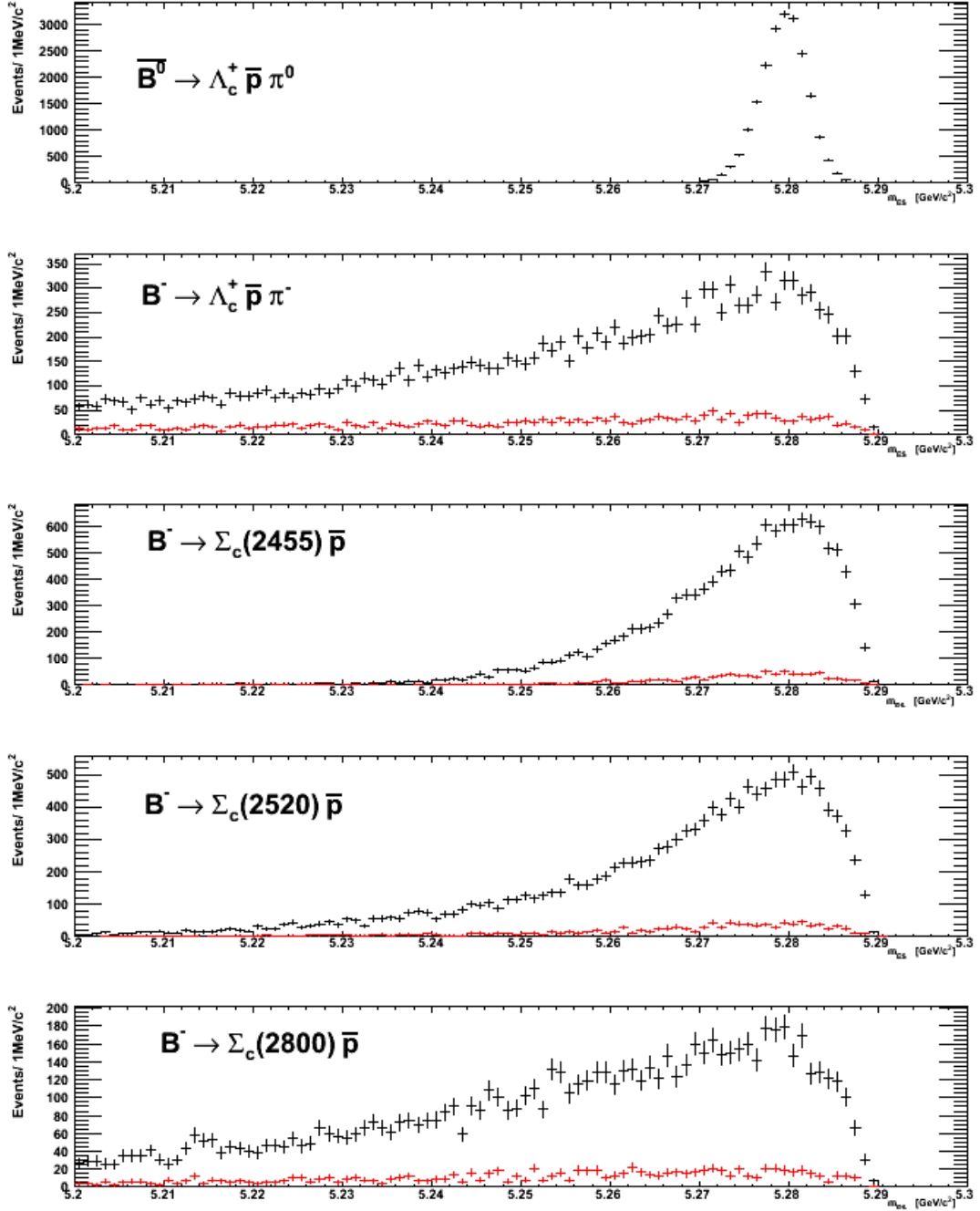


Figure 3.1: m_{ES} distributions for different MC channels (Run1-5 MC), distribution on the top is for signal MC; red data points = after veto cuts

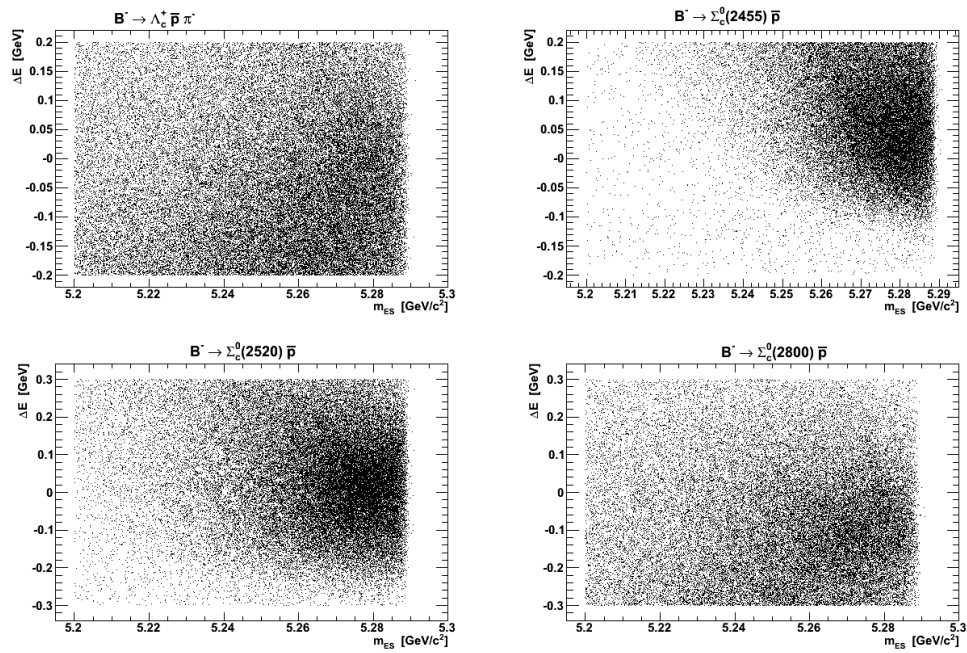


Figure 3.2: $m_{ES}:\Delta E$ distributions for different MC channels before veto cuts applied (Run1-5 MC)

3.3.3 Continuum Background

Background events consist of wrong particle combinations. This could happen in events where a B meson is created or in events where $e^+e^- \rightarrow q\bar{q}$, with $q = u, d, s$ or c . The latter one is called continuum background and in these events no B mesons could be created. To study this kind of background, data was also taken at a lower center of mass energy, too low to create B mesons (offpeak data). To see what's the fraction of continuum to the overall background after all previous cuts, we use the offpeak data and MC events processed in the same way like onpeak data, except that the energy of offpeak data is scaled to the one of onpeak data. Fig. 3.3 shows m_{ES} for onpeak data overlaid with scaled offpeak data. We can see that the fraction of continuum is the main part of the background.

We can reduce the continuum background using the thrust value which is defined as

$$T = \frac{\sum_i |\hat{T} \cdot \mathbf{p}_i|}{\sum_i |\mathbf{p}_i|} \quad (3.4)$$

where \hat{T} is the thrust axis defined as the direction which maximizes the sum of the longitudinal momenta of the particles and \mathbf{p}_i the momentum vector of the i -th particle in the center-of-mass frame. For this calculation we use all charged particles and photon candidates. The thrust is a event shape variable which describes how jet like (higher values) or how spherical (lower values) an event looks like. While continuum events are more jet like, B events are more spherical.

In fig. 3.4 the thrust distribution for signal MC and $c\bar{c}$ MC events is shown after all other selection criteria applied. To reduce the continuum background we make a selection on the thrust value of the event, $T < 0.75$. The fraction of continuum background after this additional selection criteria is shown in fig. 3.5 and the m_{ES} distribution for onpeak data overlaid with $B\bar{B}$ as well as $q\bar{q}$ MC events is shown in fig. 3.6 and describes the background in data very well. With this selection 83% of the signal remains but only 25% of the continuum background. This numbers are relative to the numbers before this selection criterion on the thrust value.

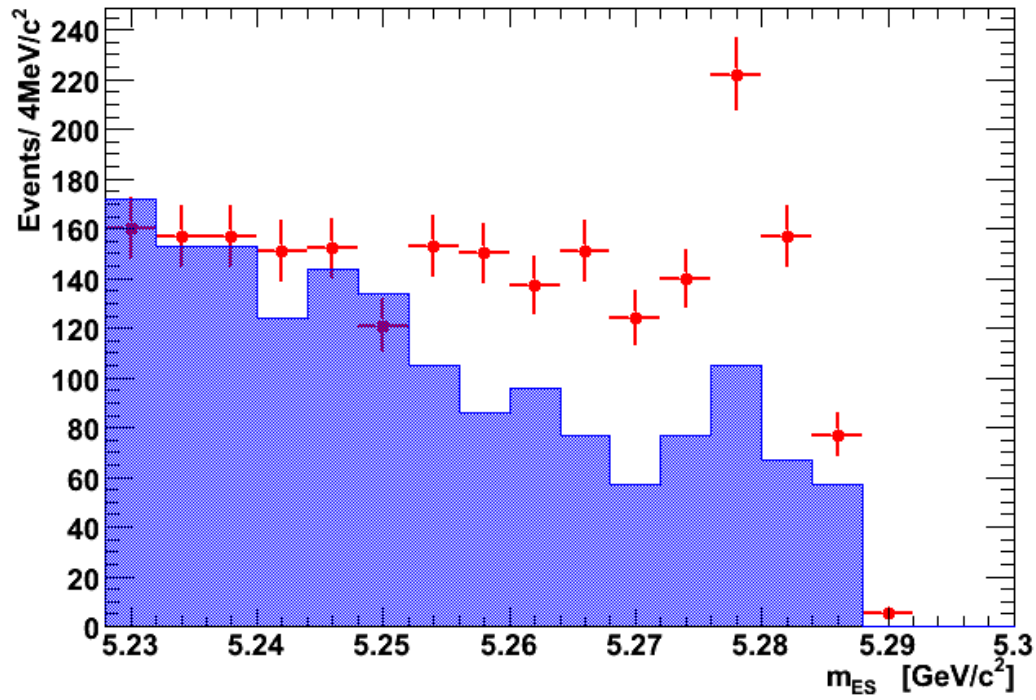


Figure 3.3: Red points are onpeak data, shaded histogram shows scaled offpeak data (before the thrust-cut).

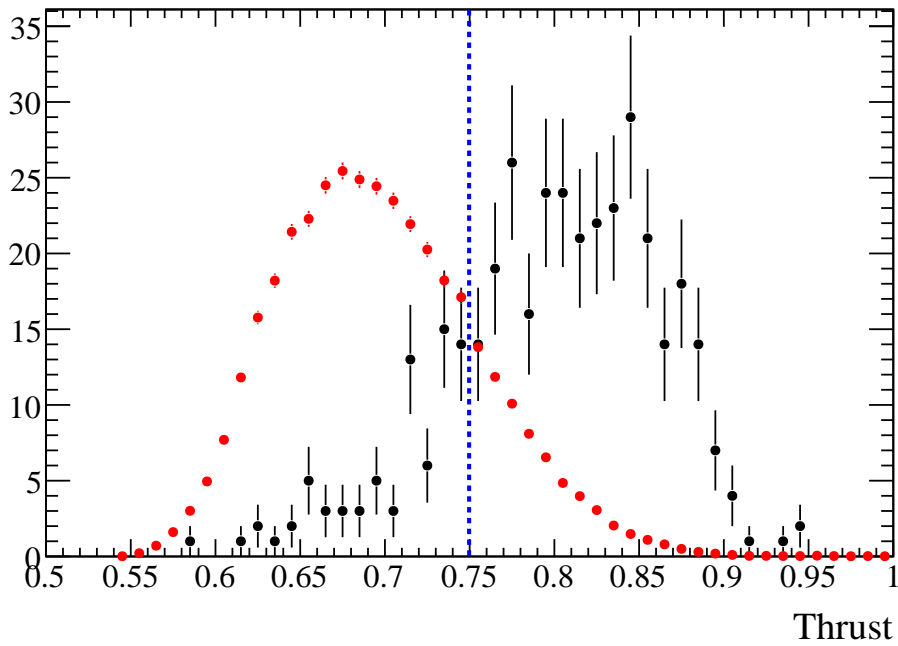


Figure 3.4: Thrust distribution for signal MC (red) and $c\bar{c}$ MC (black); the blue dashed line shows the cut value

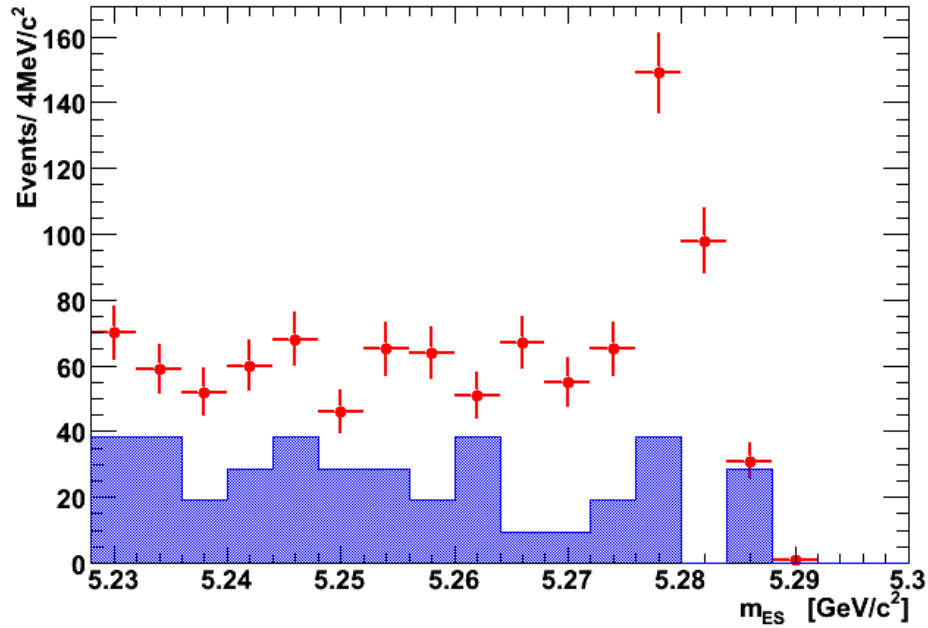


Figure 3.5: Red points are onpeak data, shaded histogram shows scaled offpeak data (after the thrust-cut).

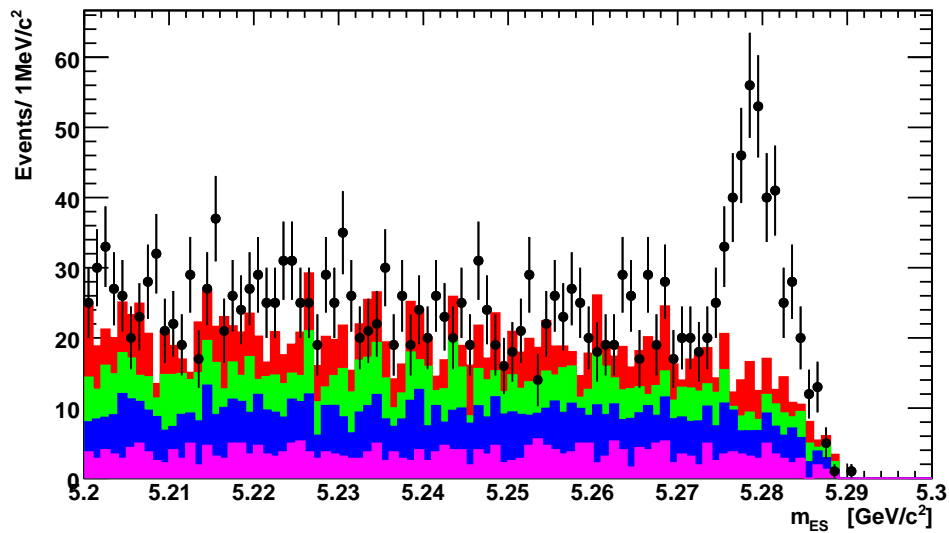


Figure 3.6: Black points are onpeak data; magenta histogram = scaled $B^0\bar{B}^0$ MC; blue histogram = scaled B^+B^- MC; green histogram = scaled $c\bar{c}$ MC; red histogram = scaled uds MC

3.3.4 Calculation of the branching fraction

After all of the previous selection criteria the number of signal candidates can be determined. We do this in the distribution of m_{ES} . For the calculation of the branching fraction we use eq. 3.5. The branching fraction for the used Λ_c^+ decay mode and the number of B mesons are known while the efficiency of the signal candidates selection, ϵ , and the number of signal candidates, N_{signal} , must be determined. To determine the number of $B^0\bar{B}^0$ pairs from the number of created $B\bar{B}$ pairs we assume $\mathcal{B}(\Upsilon(4S) \rightarrow B^0\bar{B}^0) = \mathcal{B}(\Upsilon(4S) \rightarrow B^+B^-) = 0.5$.

$$\mathcal{B}(\bar{B}^0 \rightarrow \Lambda_c^+ \bar{p} \pi^0) = \frac{N_{\text{signal}}}{\epsilon} \cdot \frac{1}{\mathcal{B}(\Lambda_c^+ \rightarrow p K^- \pi^+) \cdot 2N_{B^0\bar{B}^0}} \quad (3.5)$$

To find out which function describes best the signal distribution in m_{ES} , we study the m_{ES} distribution for MC signal events and find that the sum of two Gaussian distributions with different means (eq. 3.6) has the highest probability to describe the signal shape.

$$f(m_{\text{ES}}) = N \cdot \left((1-f) \cdot e^{-\frac{1}{2} \left(\frac{m_{\text{ES}} - m_1}{\sigma_1} \right)^2} + f \cdot e^{-\frac{1}{2} \left(\frac{m_{\text{ES}} - m_2}{\sigma_2} \right)^2} \right) \quad (3.6)$$

For the fit to the data we fix the parameters of the Gaussians to the one obtained from MC signal events fit. The combinatorial background in m_{ES} is described by the ARGUS function, eq. (3.3), and the endpoint of this function, $m_0 = 5.289 \text{ GeV}/c^2$, is fixed.

parameter	value for non efficiency corrected distribution
first mean m_1	5.2801 GeV/c^2
first width σ_1	0.0025 GeV/c^2
second mean m_2	5.2770 GeV/c^2
second width σ_2	0.0025 GeV/c^2
fraction f	0.1429

Table 3.3: fixed parameters of the signal fitting function obtained from MC signal events

Fig. 3.7 shows the m_{ES} distribution after all selection criteria. There is a clear signal and we see 273 ± 23 signal candidates in data.

To determine the significance of the signal, we assume that there is no signal and fit this distribution with the background function only. We use the likelihoods of both fits to calculate the significance, $\sqrt{-2 \ln(\mathcal{L}_0/\mathcal{L})}$, where \mathcal{L} is the likelihood of the nominal fit and \mathcal{L}_0 the likelihood value for the fit assuming there is background only. The significance of the signal is more than 10σ .

3.3.4.1 Efficiency determination

To calculate the branching fraction the efficiency still needs to be determined. This can be done by an average efficiency if MC signal events describe the data for the whole phase space. To see if this is true we can look to the invariant mass distributions for the combination of two daughter particles of the B meson. This is

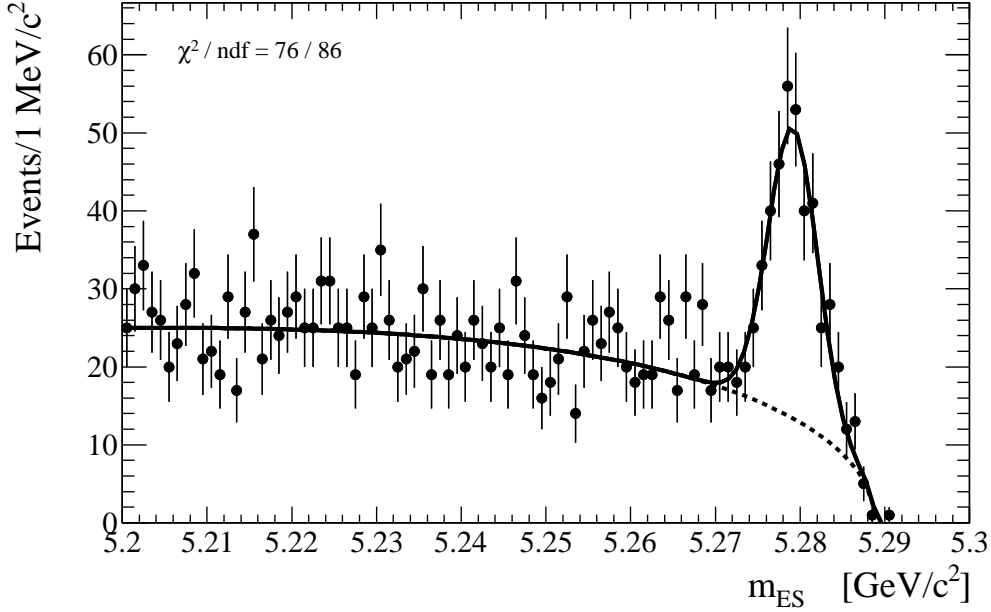


Figure 3.7: Fitted m_{ES} distribution without efficiency correction (data points); the result of the fit (solid line) and the background estimate (dashed line) is shown.

shown in figures 3.8, 3.9 and 3.10. In these figures MC events are normalized to the number of data signal events and it is shown that MC signal events don't describe the data well.

The biggest discrepancy between data and MC events is for $m(\Lambda_c^+\pi^0)$ (fig. 3.8). The differences for low invariant masses could be a hint for possible Σ_c^+ resonances but it's not really obvious from this plot because of the binning of the histogram. In this plot it should be only studied how good MC describes the data and the binning of the histogram is not small enough to show single Σ_c^+ resonances. This will be studied later. The differences for high invariant masses are a reflection from the differences in the invariant mass $m(\Lambda_c^+\bar{p})$ at low values. This is shown in fig. 3.9. The enhancement at low invariant baryon-antibaryon masses have been found in many baryonic B decays as well as totally different baryon production processes, such as $e^+e^- \rightarrow \gamma\Lambda\bar{\Lambda}$ [2][9][10][11]. The third invariant mass of the B daughter combinations is $m(\bar{p}\pi^0)$, shown in fig. 3.10. For this distribution there is a good agreement between data and MC events. For the efficiency correction an averaged efficiency for the whole phase space can not be used because MC events don't describe the data over the whole phase space. To take into account that only two invariant mass combinations are independent for a three particle final state and that MC events describe the data in one of them, the efficiency correction will be done in one dimension according to the invariant mass $m(\Lambda_c^+\pi^0)$.

To compute the efficiency the signal MC sample is divided into several intervals of $m(\Lambda_c^+\pi^0)$. For each interval the m_{ES} distribution is fitted to extract the MC signal yield. The efficiency for each interval is computed dividing this yield by the number of events generated in the interval. The resulting efficiency distribution is then fitted by a 4th order polynomial. This is shown in fig. 3.11 and the averaged signal efficiency is 6.0%.

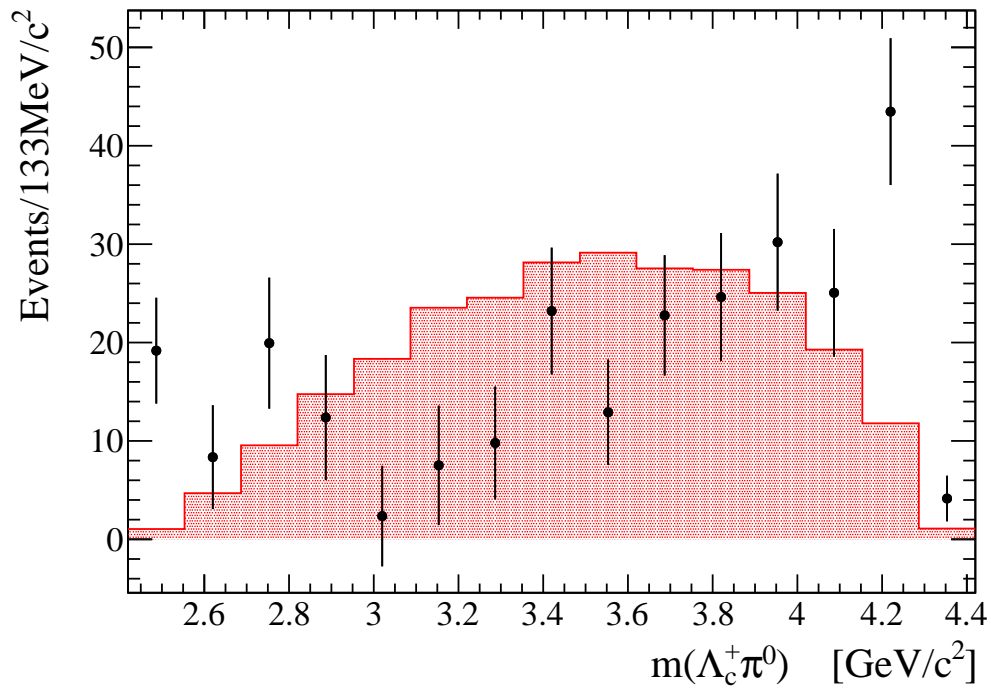


Figure 3.8: Shaded histogram shows scaled signal MC; black points are sideband subtracted data for $m_{\text{ES}} > 5.272 \text{ GeV}/c^2$; scaled to the same integral.

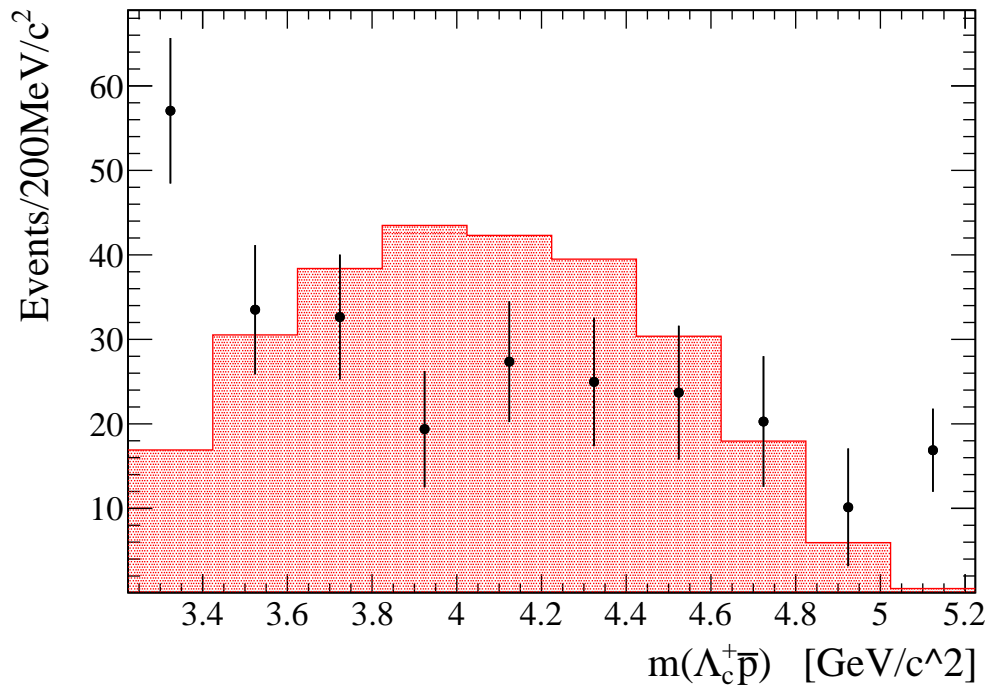


Figure 3.9: Shaded histogram shows scaled signal MC; black data points for sideband subtracted data with $m_{\text{ES}} > 5.272 \text{ GeV}/c^2$; scaled to the same integral.

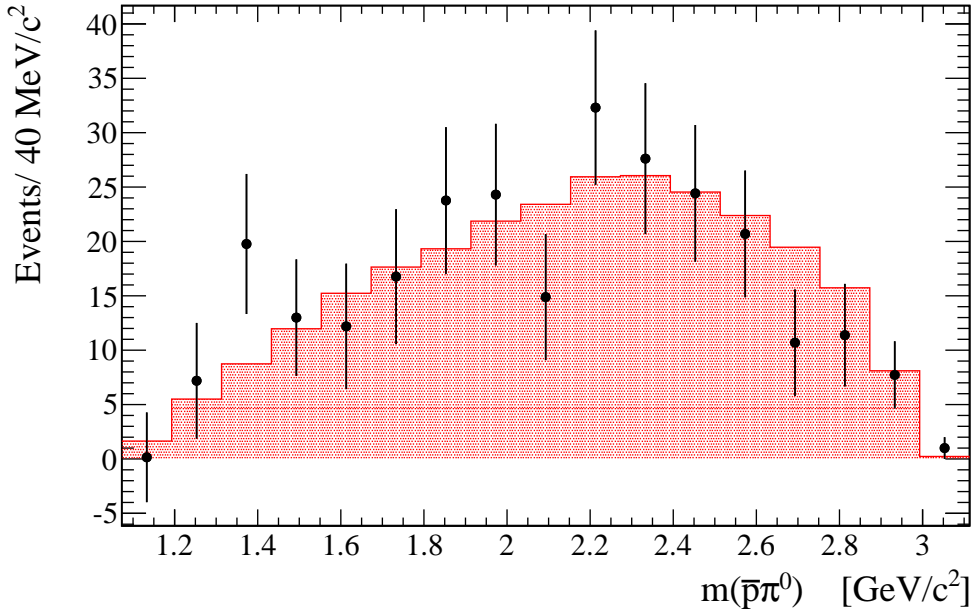


Figure 3.10: data points are for sideband subtracted signal events in data; shaded histogram shows scaled signal MC.

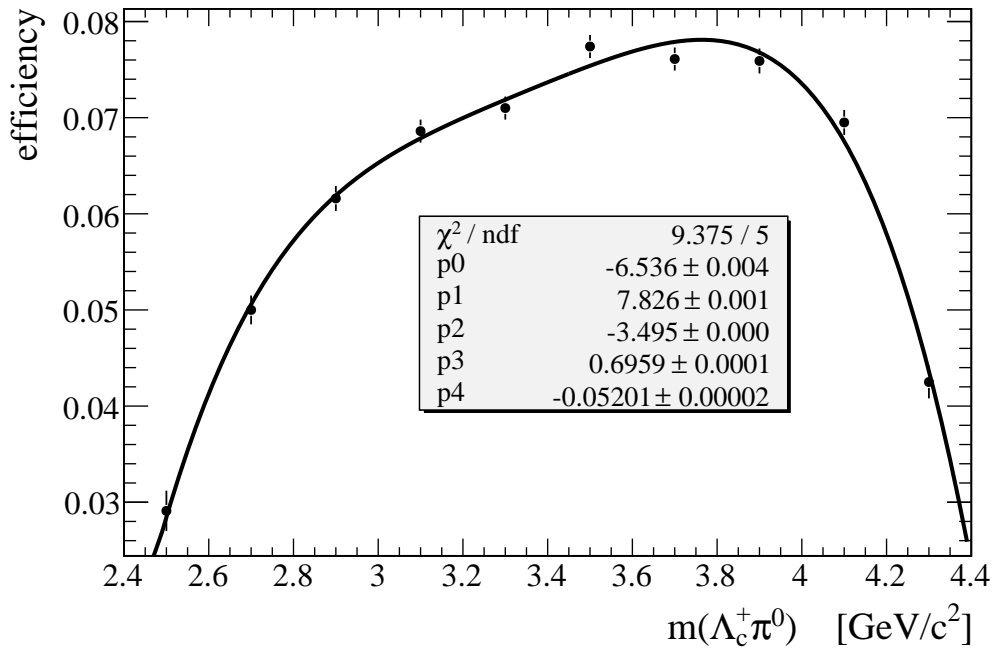


Figure 3.11: efficiency distribution fitted with a 4th order polynomial

3.3.4.2 Determination of the number of produced signal events

The number of produced signal events is given by the number of reconstructed events in data divided by the efficiency, $N_{\text{signal}}/\epsilon$. For this analysis we can not use an averaged efficiency because of the differences between MC and data events. We have to weight all events by the inverse of the efficiency given by the efficiency function. The weighted data m_{ES} distribution is shown in fig. 3.12 and fitted as

described before. This fit finds $N_{\text{produced}} = 4528 \pm 403$ signal events. The shape parameters of the signal are obtained from efficiency corrected MC (tab. 3.4) and fixed for the fit to data.

parameter	value for efficiency corrected distribution
first mean m_1	5.2799 GeV/ c^2
first width σ_1	0.0023 GeV/ c^2
second mean m_2	5.2772 GeV/ c^2
second width σ_2	0.0027 GeV/ c^2
fraction f	0.2068

Table 3.4: fixed parameters of the signal fitting function obtained from efficiency corrected MC signal events

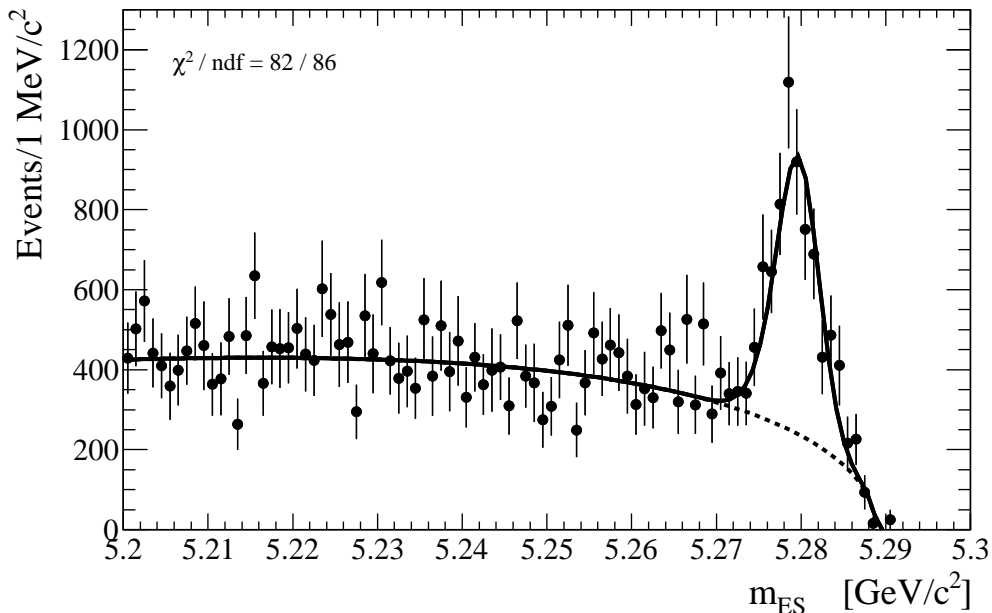


Figure 3.12: Efficiency-corrected m_{ES} distribution for $\bar{B}^0 \rightarrow \Lambda_c^+ \bar{p} \pi^0$ (data points). The result of the fit (solid line) and the background estimate (dashed line) is shown.

3.3.4.3 Branching fraction calculation

Taking into account that we weighted every event with the inverse of the efficiency for this event, eq. (3.5) changes to eq. (3.7) and the branching fraction for this B decay mode can be calculated. The uncertainty in eq. (3.7) is the statistical uncertainty only.

$$\mathcal{B}(\bar{B}^0 \rightarrow \Lambda_c^+ \bar{p} \pi^0) = \frac{N_{\text{produced}}}{\mathcal{B}(\Lambda_c^+ \rightarrow p K^- \pi^+) \cdot 2N_{B^0 \bar{B}^0}} = (1.94 \pm 0.17) \times 10^{-4} \quad (3.7)$$

3.3.5 Cross checks

To be sure that the signal is made by real π^0 and Λ_c^+ , it is necessary to look into the invariant mass distributions for these candidates. To be able to do this a new data

sample was generated without constraining the mass of the Λ_c^+ and π^0 candidate and the m_{ES} distribution without efficiency correction is fitted like before. The fit to this m_{ES} distribution finds 254 ± 22 signal events.

For the signal distributions of the daughter particles a sideband subtraction is used. The mass distributions are created for the signal region, $5.272 < m_{ES} < 5.286 \text{ GeV}/c^2$, and for a sideband region, $5.240 < m_{ES} < 5.260 \text{ GeV}/c^2$. The one for the sideband region is scaled to the expected number of background events in the signal region and subtracted from the distribution for the signal region. The scaling factor is given by the integral of the fitted ARGUS function in the sideband and signal region. If the signal in m_{ES} is made by real π^0 and Λ_c^+ candidates the sideband subtracted mass distributions can be described by a signal function only and the fit with this function to the mass distribution will find the same number of signal candidates like the fit to the m_{ES} distribution.

The invariant mass distribution for the π^0 signal candidates is shown in fig. 3.13. The fit describing the signal with a Crystal ball function ([12]) finds 259 ± 25 π^0 candidates. In fig. 3.14 the invariant mass distribution for Λ_c^+ signal candidates is fitted with a Gaussian. This fit finds 269 ± 24 signal candidates. Simple counting of events in both histograms leads to 251 π^0 and 255 Λ_c^+ signal candidates. From this plots it can be seen that the reconstruction of the daughter particles works and that the signal candidates found in m_{ES} are made by real π^0 and Λ_c^+ candidates.

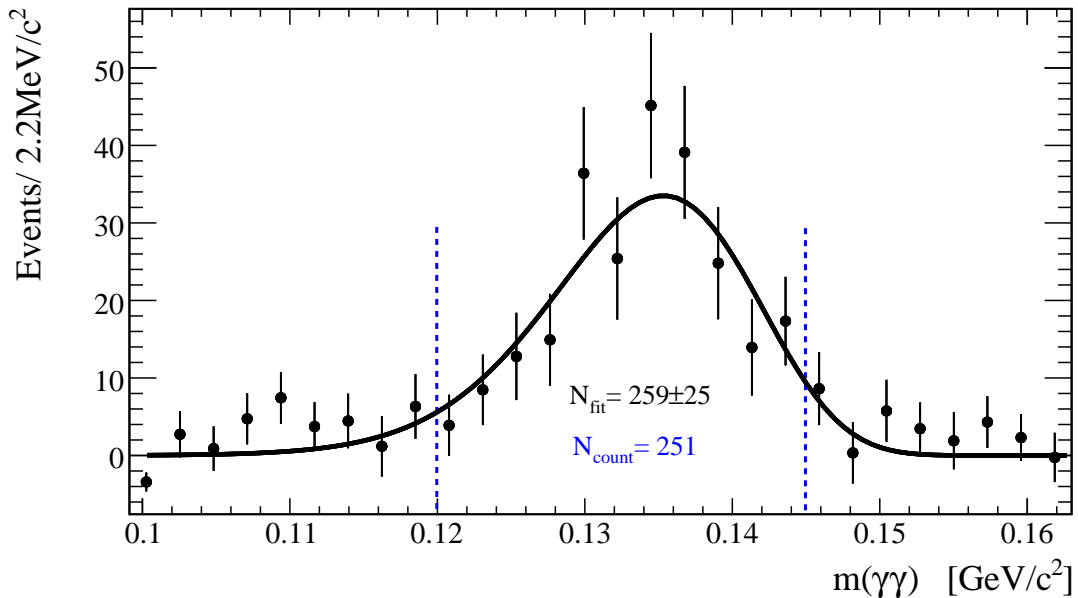


Figure 3.13: distribution of sideband subtracted data events fitted with a Crystal Ball function; blue lines show the cuts on $m(\gamma\gamma)$ for the default analysis.

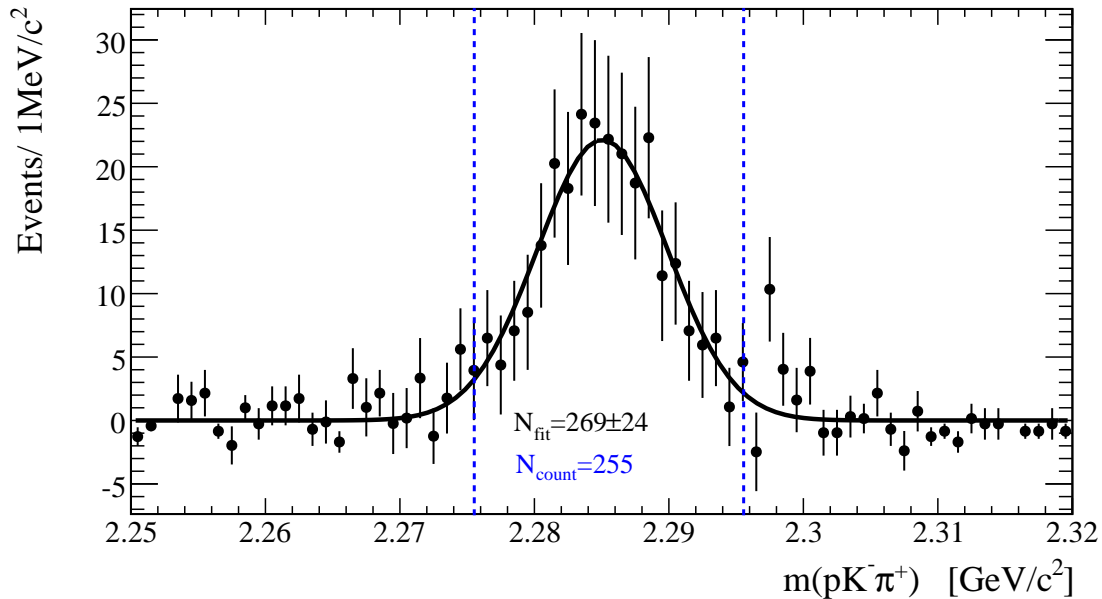


Figure 3.14: distribution of sideband subtracted data events fitted with a Gaussian; blue lines show the cuts on $m(pK^-\pi^+)$ for the default analysis.

3.3.6 Resonances

3.3.6.1 $\Lambda_c^+ \pi^0$ resonant states

We have seen in subsection 3.3.4 that there is a discrepancy between MC and data signal events for the invariant mass distributions $m(\Lambda_c^+ \pi^0)$ and $m(\Lambda_c^+ \bar{p})$. To see if this is due to some resonant sub modes, like $\bar{B}^0 \rightarrow \Sigma_c^+ \bar{p}, \Sigma_c^+ \rightarrow \Lambda_c^+ \pi^0$, these distributions will be studied again. There are three Σ_c^+ resonances known, while the one with the lowest mass and smallest width, the $\Sigma_c(2455)$, shows up in all B decay modes with a Σ_c in the final state. The mass of the $\Sigma_c(2455)$ is about $2.455 \text{ GeV}/c^2$. To be able to see this resonance in data we have to use a finer binning of the histogram shown in fig. 3.8 (fig. 3.15). But if we do so, then there is no structure visible. However, we can still use it to calculate an upper limit for the decay mode $\bar{B}^0 \rightarrow \Sigma_c^+(2455) \bar{p}$. This resonance is near the lower phase space border so the expected combinatorial background is very low. This is not true for the other Σ_c resonances with higher masses. That's why we calculate only the upper limit for the B decay to the $\Sigma_c^+(2455)$ resonance.

In Fig. 3.15, the invariant mass of the $\Lambda_c^+ \pi^0$ combination is shown which is fitted by a Gaussian function for a possible $\Sigma_c^+(2455)$ signal and by the function $n \times (m(\Lambda_c^+ \pi^0) - [m(\Lambda_c^+) + m(\pi^0)])^c$ to describe the non-resonant fraction of the signal and background using a likelihood fit. The shape parameters for the Gaussian are fixed to the parameters obtained from simulated events. The fit returns $N = 3 \pm 3$ signal events. The reconstruction efficiency for $\bar{B}^0 \rightarrow \Sigma_c^+(2455) \bar{p}$ is $\epsilon_{\Sigma_c^+(2455)} = (1.70 \pm 0.05)\%$. To obtain a Bayesian upper limit at 90% confidence level (C.L.) we have to integrate the likelihood function of the fit parameter $N \geq 0$.

Fig. 3.16 shows the Likelihood distribution for the fit parameter N . Integrating this distribution gives $N_{\text{UL}} = 11$ corresponding to a 90% C.L. upper limit of the

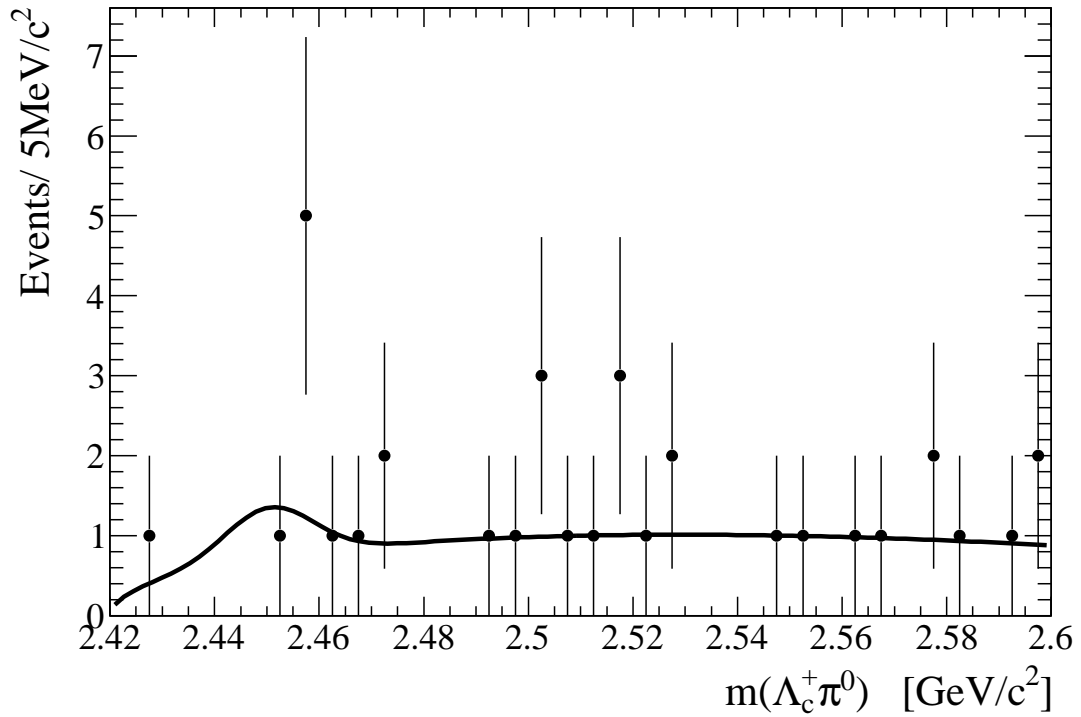


Figure 3.15: Distribution of the invariant mass of the $\Lambda_c^+ \pi^0$ system in the region where the $\Sigma_c^+(2455)$ resonance is expected; points are for data within the m_{ES} signal region, the curve shows the fit.

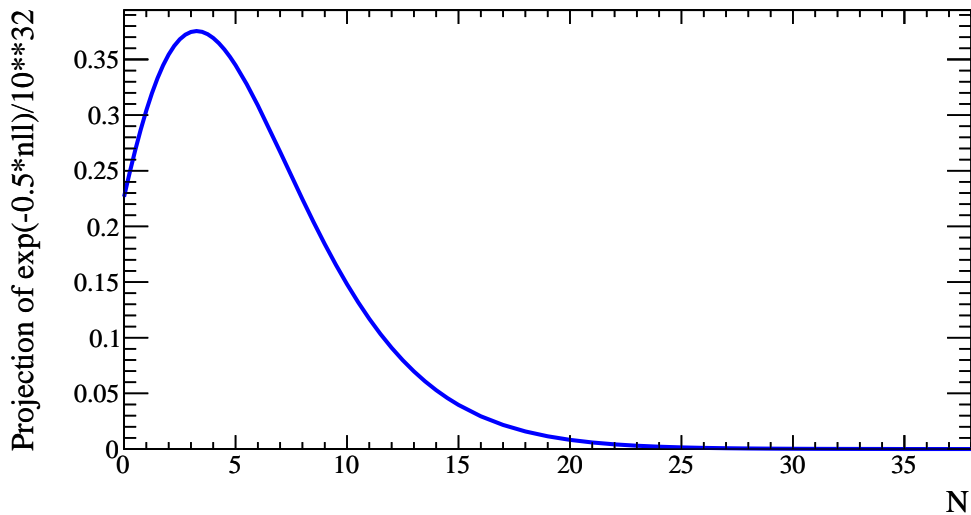


Figure 3.16: Likelihood distribution for the number of signal events from the fit in fig. 3.15

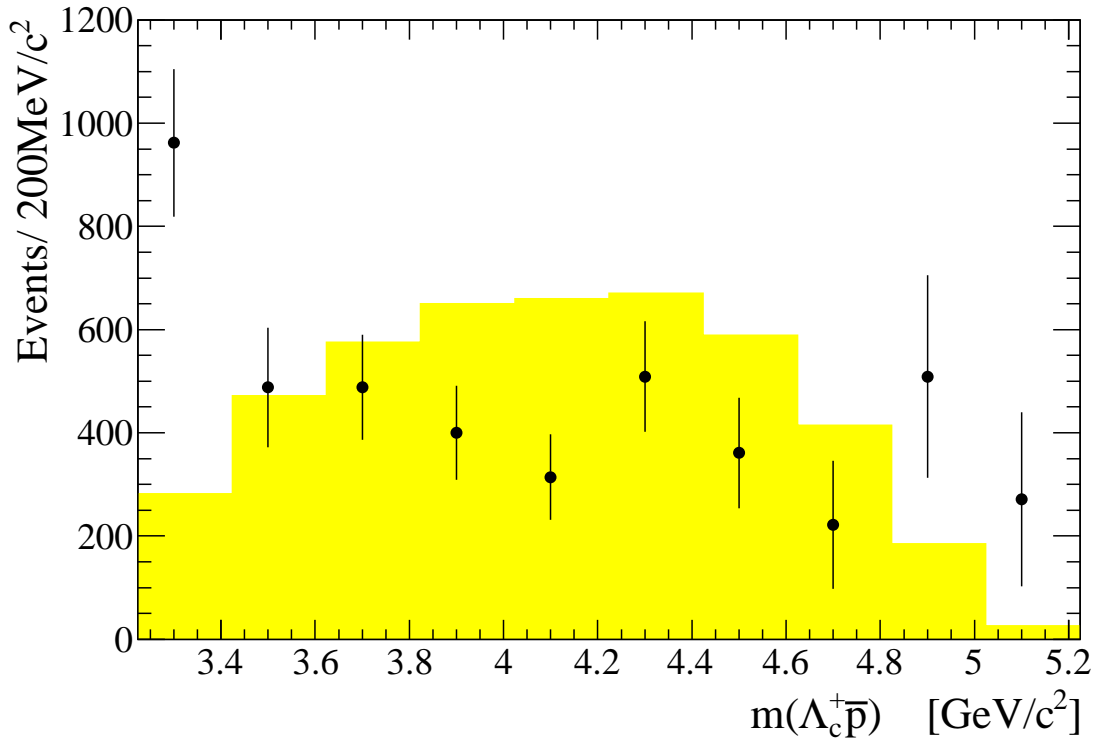


Figure 3.17: Efficiency corrected distribution of the invariant mass $m(\Lambda_c^+ \bar{p})$; points are signal data events; histogram shows signal MC events assuming a phase space distribution normalized to the number of data events.

branching fraction. Using eq. (3.5) we are able to calculate the upper limit for the branching fraction now. Due to the big systematic uncertainty on the Λ_c^+ branching fraction we calculate the combined branching fraction in eq. (3.8).

$$\mathcal{B}(\bar{B}^0 \rightarrow \Sigma_c^+(2455) \bar{p}) \times \mathcal{B}(\Lambda_c^+ \rightarrow p K^- \pi^+) < \frac{N_{\text{UL}}}{\epsilon_{\Sigma_c^+(2455)}} \cdot \frac{1}{2 \cdot N_{B^0 \bar{B}^0}} = 1.5 \times 10^{-6} \quad (3.8)$$

3.3.6.2 $\Lambda_c^+ \bar{p}$ mass distribution

In many baryon production processes an enhancement at threshold of the invariant baryon-antibaryon mass has been found. This could be a hint of the production mechanism for baryons. In production processes where it's not possible that the invariant mass of the baryon-antibaryon system is low, like $\bar{B}^0 \rightarrow \Lambda_c^+ \bar{p}$, the branching fraction is much lower than for comparable processes, like $B^- \rightarrow \Lambda_c^+ \bar{p} \pi^-$, where $m(\Lambda_c^+ \bar{p}) = m(\Lambda_c^+) + m(\bar{p})$ is possible [2].

In contrast to the mass distribution for $m(\Lambda_c^+ \pi^0)$ where we only wanted to calculate the upper limit for one resonant state, we want to know how the whole mass distribution $m(\Lambda_c^+ \bar{p})$ looks like. Given that we have seen that the efficiency varies a lot across the phase space we have to weight all events with the inverse of the efficiency again. To extract the signal from the background we divide the data sample into 10 intervals of $m(\Lambda_c^+ \bar{p})$ and fit in every interval the efficiency-corrected m_{ES} distribution. The signal yield for every interval is shown in fig. 3.17 together with MC

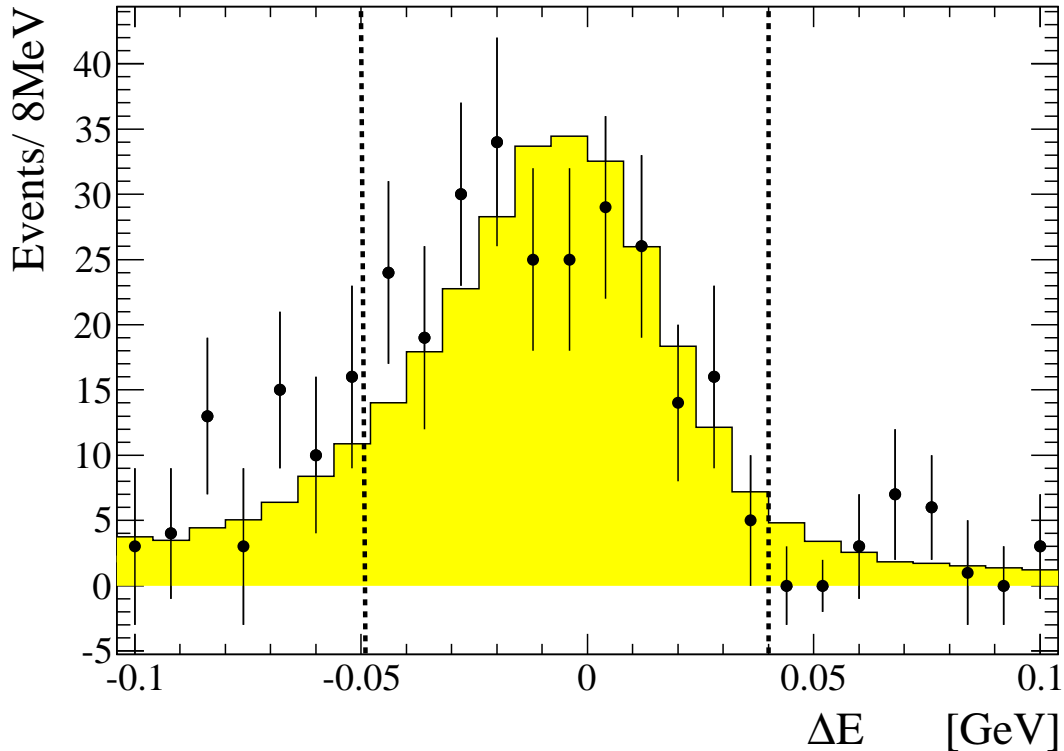


Figure 3.18: ΔE distribution for data signal events after all selection cuts (data points) and signal MC events (histogram) normalized to the number of data signal events; signal events are obtained from binwise m_{ES} fits; dashed lines show the range used for m_{ES} distributions.

signal events, generated with a phase space distribution for the B decay to $\Lambda_c^+ \bar{p} \pi^0$. The MC signal events are normalized to the number of data events over the whole phase space. There is a difference in the shape between data and simulation. We can also see a clear enhancement at low mass, with a significance of 5σ for the first bin, assuming Gaussian statistics.

3.3.7 Systematic uncertainties

To derive the systematic uncertainties data control samples are studied, data and MC events are compared and the parameters of the fit are varied.

We have to compare for all distributions we make selections on, whether MC events describe the data or not. While the distributions derived from MC events describe the data very well for most variables, there is a difference for the ΔE distribution. This is shown in fig. 3.18, where the m_{ES} distribution was fitted in every interval of ΔE . To take this difference in the shape into account we can use the difference between the cut efficiency in MC and data events, relative to the MC one, as the systematic uncertainty. It is 4.6%.

For the fit to m_{ES} itself the fixed parameters have been varied and also the range of the fit. The number of signal candidates found with the new fit can be compared with the number of the default fit. The difference in this number of signal candidates is for all parameters very low and we can use the largest variance found for the fit

systematic uncertainty. The largest difference was found for varying the end point of the ARGUS function by $1 \text{ MeV}/c^2$ and the associated uncertainty is 0.5%.

To determine the uncertainty due to the used MC model we use to generate signal events, we can reweight the signal events depending on $m(\bar{p}\pi^0)$. A new efficiency function must be calculated and the events corrected for reconstruction efficiencies with this new function. The fit to this efficiency corrected m_{ES} distribution will find a different number of signal events and we can use the difference to the default fit as the uncertainty associated with the used MC model (2.2%).

Other uncertainties arise from the veto cuts (3.4%), the π^0 reconstruction efficiency (3.0%), the particle identification (1.2%), the number of $B^0\bar{B}^0$ pairs (1.1%) and the reconstruction efficiency of charged tracks (0.9%). The systematic uncertainty on the veto cuts are obtained from the difference of signal selection with and without this selection criteria, while all other uncertainties are provided by different working groups at *BABAR*.

All individual contributions are added in quadrature, resulting in the total of 7.1%. All sources of systematic uncertainties are summarized in tab. 3.5.

Source	value
differences between MC and data	4.6%
veto cuts	3.4%
π^0 reconstruction	3.0%
used MC model	2.2%
particle identification	1.2%
number of $B^0\bar{B}^0$	1.1%
reconstruction eff. of charged tracks	0.9%
fixed fit parameter	0.5%
total	7.1%

Table 3.5: Systematic uncertainties for the reconstruction of $\bar{B}^0 \rightarrow \Lambda_c^+ \bar{p} \pi^0$

3.4 Reconstruction of $\bar{B}^0 \rightarrow \Lambda_c^+ \bar{p} \eta$

For the reconstruction of this B decay mode we use only $\eta \rightarrow \gamma\gamma$ which has a branching fraction of $(39.31 \pm 0.20)\%$ [3]. We will use all the selection criteria and reconstruction techniques, like the geometric constraint fit, described in sec. 3.3, except the one for the photons and π^0 . We will also use the same selection method of one candidate per event. This ensures that most of the systematics will cancel in the ratio $\mathcal{B}(\bar{B}^0 \rightarrow \Lambda_c^+ \bar{p} \pi^0)/\mathcal{B}(\bar{B}^0 \rightarrow \Lambda_c^+ \bar{p} \eta)$. All MC modes listed in tab. 3.1 and tab. 3.2 are analysed again and we haven't found any other mode which could contribute to the signal. So there is no peaking background for the reconstruction of the decay mode with the η in the final state and we don't need the veto cuts.

3.4.1 Selection Criteria

The selection of the η candidate should maximize the signal significance again. All cuts from the optimization process as well as from the previous analyses are:

- charged tracks must origin within 1.5cm of the beam spot in the xy-plane and within 2.5cm in the z-direction
- no PID list used for π^- identification; all charged tracks are used as pion candidates
- PID lists using Likelihood selectors for particle identification with the following criteria are used :
 - protons from Λ_c^+ must fullfil: $\frac{L_p}{L_K+L_p} > 0.7000$, $\frac{L_p}{L_p+L_\pi} > 0.5000$ and must not be in a predefined electron list if they have momentum higher than 0.7 GeV/c
 - Kaons from Λ_c^+ must fullfil: $\frac{L_K}{L_K+L_\pi} > 0.8176$, $\frac{L_K}{L_p+L_K} > 0.0180$ and must also no be in a predefined electron list if they have a momentum higher than 0.4 GeV/c
 - protons from the \bar{B}^0 must fullfil: $\frac{L_p}{L_K+L_p} > 0.25$, $\frac{L_p}{L_p+L_\pi} > 0.5000$
- $2.276 < m(pK^-\pi^+) < 2.296$ GeV/ c^2 (within 2.5σ of the fitted peak of the mass distribution)
- Probability for $(p K^- \pi^+)$ vertex fit > 0.001
- $E(\gamma_1) > 0.14$ GeV
- $E(\gamma_2) > 0.40$ GeV (it's always: $E(\gamma_1) < E(\gamma_2)$)
- $0.52 < m(\gamma\gamma) < 0.56$ GeV/ c^2 for the η candidate
- Probability for B_{cand} fit > 0.001 (fit to common vertex and using mass constraints for π^0 and Λ_c^+ candidates)
- $0.06 < \Delta E < 0.03$ GeV/ c^2

In fig. 3.19 the data distribution is shown together with the expected combinatorial $B\bar{B}$ and continuum background, taken from MC events. We can see that there is again a good agreement between the expected background from MC simulation and the data outside of the signal region and a clear signal around $m_{\text{ES}} = 5.279$ GeV/ c^2 in the data events but not in the simulated events.

3.4.2 Calculation of the branching fraction

For the calculation of the branching fraction we choose to go the same way as for the π^0 decay mode. The extraction of the number of signal candidates will be done again in the efficiency corrected m_{ES} distribution using a fit with the same functions to describe signal and background as before. The parameters shown in tab. 3.6 are obtained from a fit to simulated signal events and fixed for the fit to data.

Fig. 3.20 shows the fit to data after all selection criteria applied. There is a signal visible and we see 53 ± 12 signal candidates in data. To calculate the significance we also have to fit this distribution with the background function only. From the Likelihoods of both fits we can calculate the significance, which is 4.6σ .

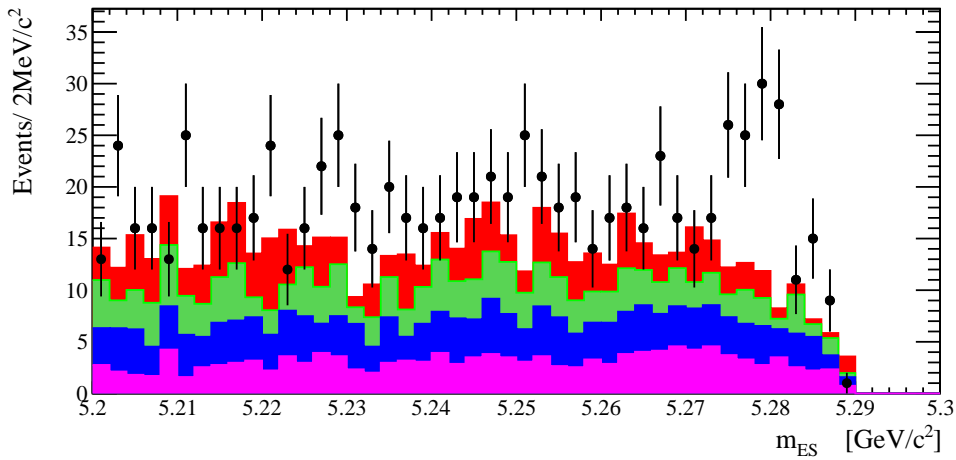


Figure 3.19: Black points are onpeak data; magenta histogram = scaled $B^0 \bar{B}^0$ MC; blue histogram = scaled $B^+ B^-$ MC; green histogram = scaled $c\bar{c}$ MC; red histogram = scaled uds MC

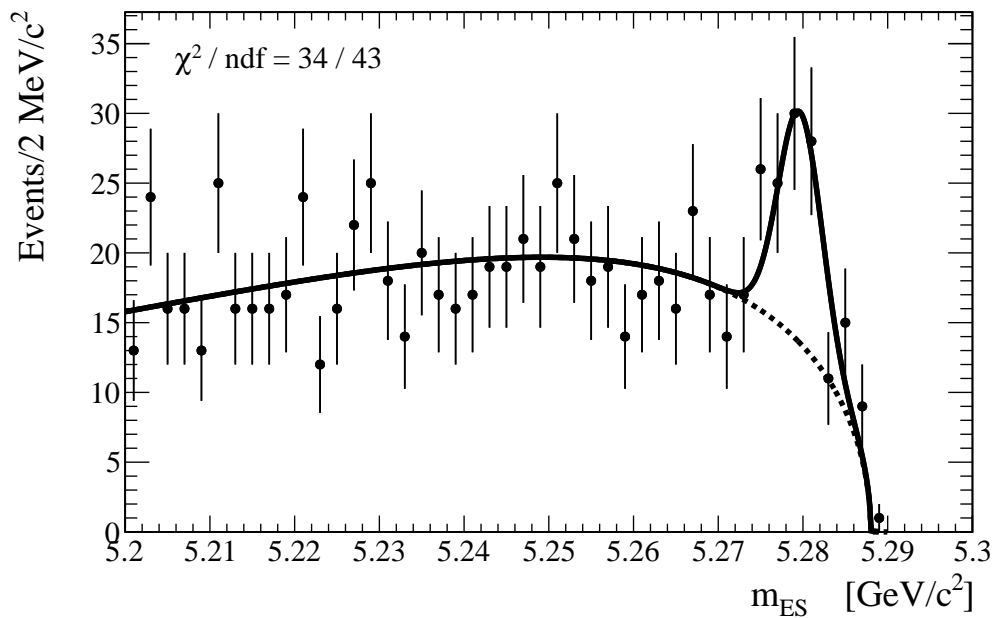


Figure 3.20: Fitted m_{ES} distribution without efficiency correction (data points); the result of the fit (solid line) and the background estimate (dashed line) is shown.

parameter	value for non efficiency corrected distribution
first mean m_1	5.2797 GeV/c ²
first width σ_1	0.0026 GeV/c ²
second mean m_2	5.2769 GeV/c ²
second width σ_2	0.0048 GeV/c ²
fraction f	0.0026

Table 3.6: fixed parameters of the signal fitting function obtained from MC signal events

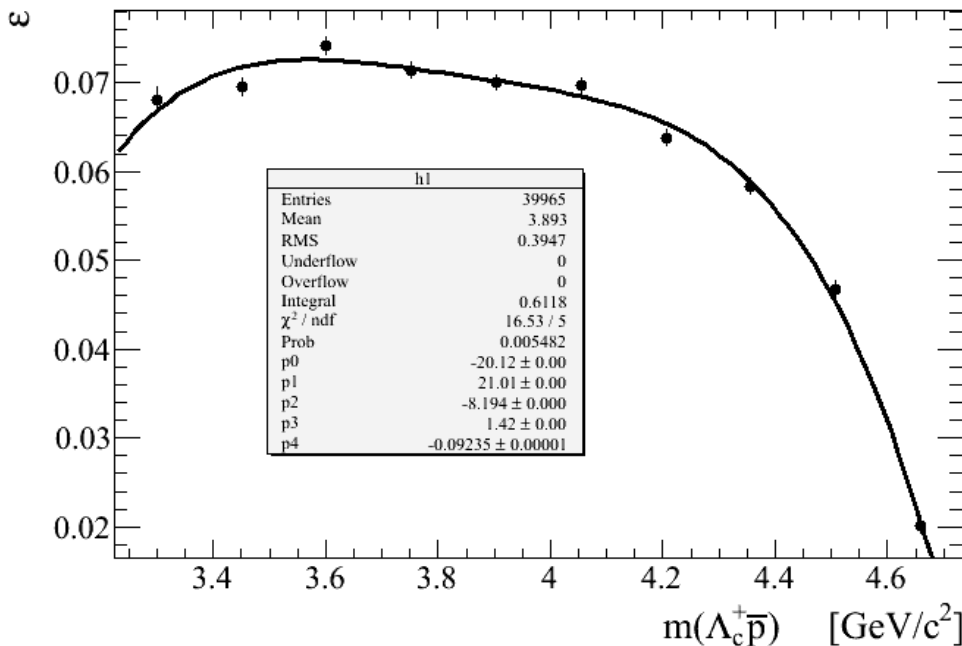


Figure 3.21: Efficiency distribution in bins of $m(\Lambda_c^+ \bar{p})$ fitted with a 4th order polynomial.

3.4.2.1 Efficiency determination

For this decay mode we do the efficiency correction in bins of $m(\Lambda_c^+ \bar{p})$.

We divide our data sample into 10 intervals of $m(\Lambda_c^+ \bar{p})$ and fit the m_{ES} distribution as described before for every interval. Then the extracted signal yield is divided by the number of generated events in every interval which gives the efficiency. We fit the resulting efficiency distribution with a 4th order polynomial. This is shown in fig. 3.21.

3.4.2.2 Determination of the number of produced signal events

We use the same way as for the π^0 decay mode. To determine the number of produced events we weight all events with the inverse of the efficiency according to the efficiency function in fig. 3.21. The resulting m_{ES} distribution (fig. 3.22) is then fitted again as described before and we find 866 ± 260 signal events. For this fit the shape parameters of the signal function are fixed to the values obtained from a fit to efficiency corrected signal MC events (tab. 3.7).

parameter	value for efficiency corrected distribution
first mean m_1	5.2797 GeV/c ²
first width σ_1	0.0026 GeV/c ²
second mean m_2	5.2759 GeV/c ²
second width σ_2	0.0059 GeV/c ²
fraction f	0.0603

Table 3.7: fixed parameters of the signal fitting function obtained from efficiency corrected MC signal events

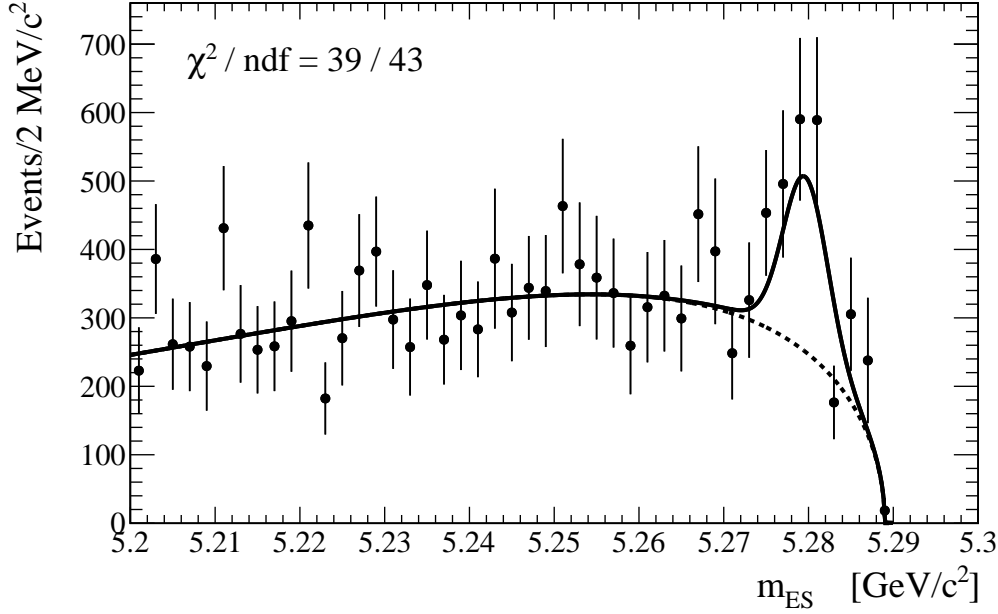


Figure 3.22: Efficiency-corrected m_{ES} distribution ; the result of the fit (solid line) and the background estimate are shown.

3.4.2.3 Branching fraction calculation

The branching fraction for this decay mode could be calculated with the following numbers:

- $N_{B^0\bar{B}^0} = (233.6 \pm 0.06) \times 10^6$
- $\mathcal{B}(\Lambda_c^+ \rightarrow pK^-\pi^+) = (5.0 \pm 1.3)\%$
- $\mathcal{B}(\eta \rightarrow \gamma\gamma) = (39.31 \pm 0.20)\%$
- $N_{\text{produced}} = 866 \pm 260$,

where the uncertainties for $N_{B\bar{B}}$ and N_{produced} are statistical only. We calculate the branching fraction using eq. (3.9) and find $\mathcal{B}(\bar{B}^0 \rightarrow \Lambda_c^+ \bar{p} \eta) = (0.94 \pm 0.28) \times 10^{-4}$, where the uncertainty is statistical only.

$$\mathcal{B}(\bar{B}^0 \rightarrow \Lambda_c^+ \bar{p} \eta) = \frac{N_{\text{produced}}}{\mathcal{B}(\Lambda_c^+ \rightarrow pK^-\pi^+) \cdot \mathcal{B}(\eta \rightarrow \gamma\gamma) \cdot 2N_{B^0\bar{B}^0}} = (0.94 \pm 0.28) \times 10^{-4} \quad (3.9)$$

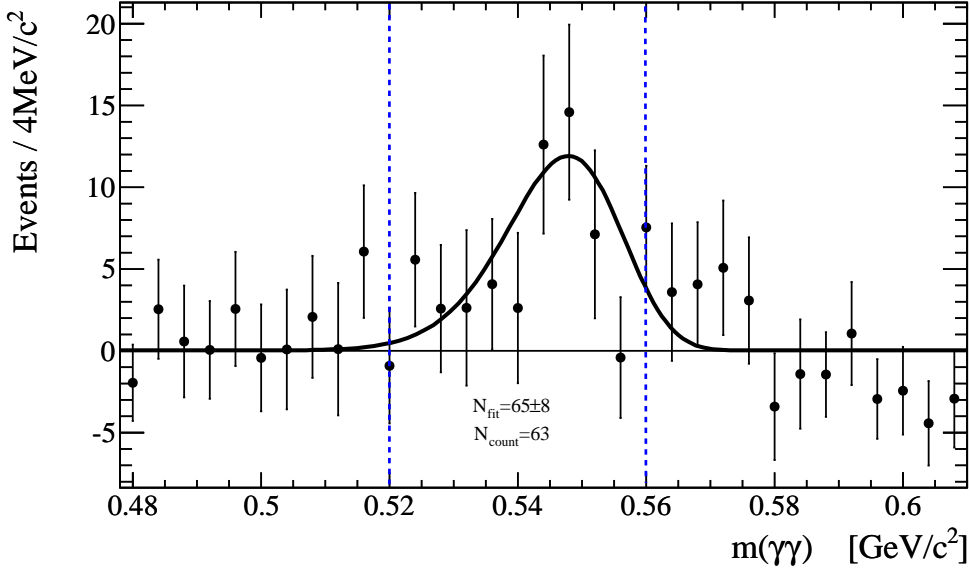


Figure 3.23: Distribution of sideband subtracted data events fitted with a Novosibirsk function $f \sim e^{-\frac{1}{2}\left(\frac{\ln^2[1+\Lambda\tau\cdot(m(\gamma\gamma)-\mu)]}{\tau^2} + \tau^2\right)}$ and $\Lambda = \sinh(\tau\sqrt{\ln 4})/(\sigma\tau\sqrt{\ln 4})$ where μ is the mean, σ the width and τ the asymmetry of this function; blue lines show the cut range for $m(\gamma\gamma)$.

3.4.3 Cross checks

Like for the other analyzed decay mode we look into the invariant mass distribution for η and Λ_c^+ candidates made from a data sample without a mass constraint applied. The fit to the m_{ES} distribution based on this data sample finds 52 ± 12 signal events. For the invariant mass distributions (fig. 3.23 and fig. 3.24) we use the same sideband subtraction as described in the other analysis. The fit to $m(\gamma\gamma)$ finds 65 ± 8 signal events and the fit to $m(pK^-\pi^+)$ 50 ± 14 signal events. Given that there should be only m_{ES} signal candidates in the invariant mass distributions we can also sum up the signal candidates for every bin. Counting the number of η candidates results in 63 and for Λ_c^+ candidates in 51. All numbers are consistent with each other.

3.4.4 Two-body mass distributions

Due to the limited statistics we are not able to fit the efficiency corrected m_{ES} distribution in every bin of the different mass distributions. For this reason we will use a sideband subtraction as described before.

The mass distribution $m(\bar{p}\eta)$ in fig. 3.25 shows a good agreement between signal data events and phase space generated signal MC events. In fig. 3.26 the invariant mass distribution for $m(\Lambda_c^+\bar{p})$ is shown. In difference to the decay mode $\bar{B}^0 \rightarrow \Lambda_c^+\bar{p}\pi^0$ and many other baryonic B -decays, there is no enhancement at threshold but for high values of the invariant two-body mass. This could be a hint of a different decay mechanism compared with the other analyzed B -decay mode. The invariant mass distribution for $m(\Lambda_c^+\eta)$ (fig. 3.27) shows a large difference to the phase space generated signal MC events at threshold. This could be a reflection from $m(\Lambda_c^+\bar{p})$ or maybe a resonance at low $m(\Lambda_c^+\eta)$. But due to the limited statistics we are not able to fit the efficiency corrected m_{ES} in more bins than we did.

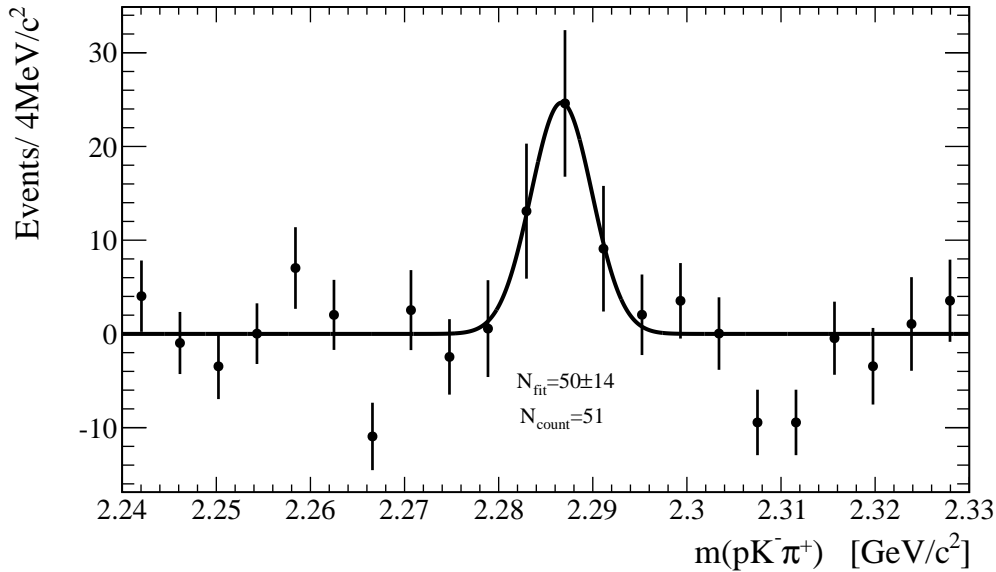


Figure 3.24: Distribution of sideband subtracted data events fitted with a Gaussian.

We see that phase space generated MC signal events agree with data in one of the three possible invariant two-body mass distributions and therefore we can do the efficiency correction in one of the two other distributions, as we did.

3.4.5 Systematic uncertainties

For the systematic uncertainties we consider the same sources like for the other decay mode. A list of all sources could be found in tab. 3.8. When we compare the distribution of all variables we cut on in data and MC, we find again only for the ΔE distribution a difference. But compared with the π^0 mode it's much smaller for this decay mode (2%) due to the higher energy of the photons which could be better simulated. The highest systematic uncertainty comes from the variation of the fit parameters because the statistics is much lower than for the π^0 decay mode and therefore even a small variation of the fit parameters could have a bigger impact on the fit result. The variation of the ARGUS end point by 1 MeV/ c^2 gives the highest variation of the number of signal candidates (3.7%).

Source	value
fixed fit parameter	3.7%
η reconstruction	3.0%
differences between MC and data	2.0%
used MC model	1.3%
particle identification	1.2%
number of $B^0\bar{B}^0$	1.1%
reconstruction eff. of charged tracks	0.9%
total	5.6%

Table 3.8: Systematic uncertainties for the reconstruction of $\bar{B}^0 \rightarrow \Lambda_c^+ \bar{p} \eta$

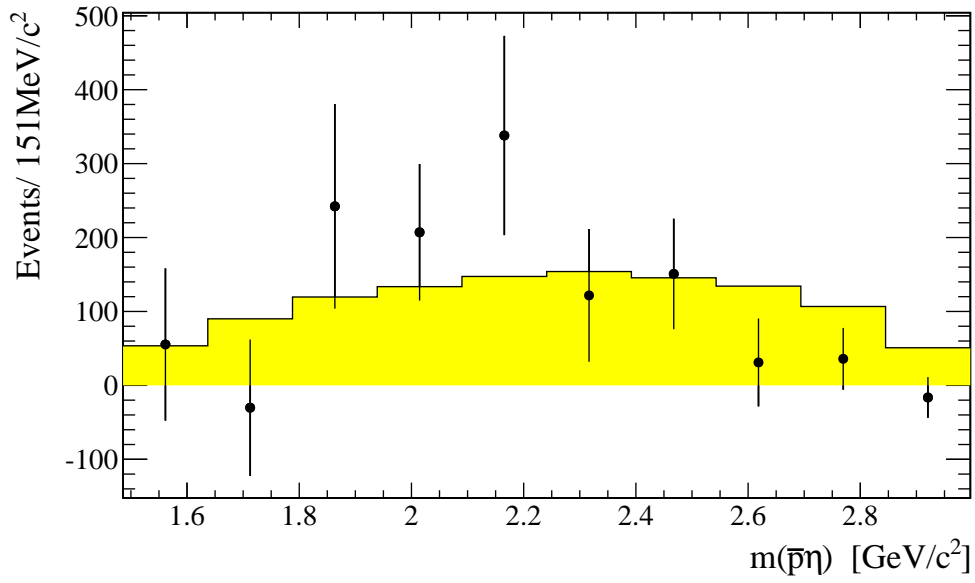


Figure 3.25: Efficiency corrected distribution of sideband subtracted signal data events (data points) and phase space generated MC signal events (histogram) for $m(\bar{p}\eta)$; scaled to the same integral.

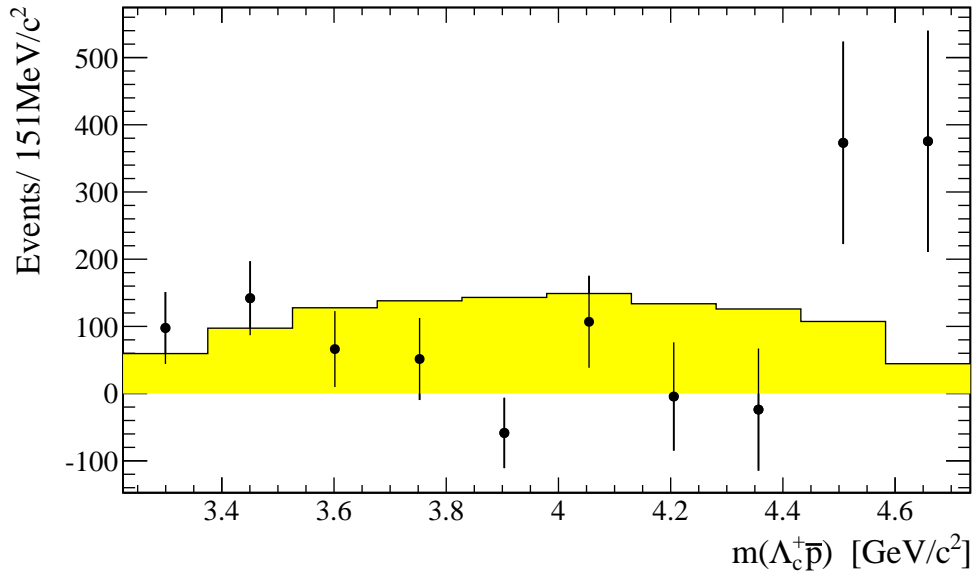


Figure 3.26: Efficiency corrected distribution of sideband subtracted signal data events (data points) and phase space generated MC signal events (histogram) for $m(\Lambda_c^+\bar{p})$; scaled to the same integral.

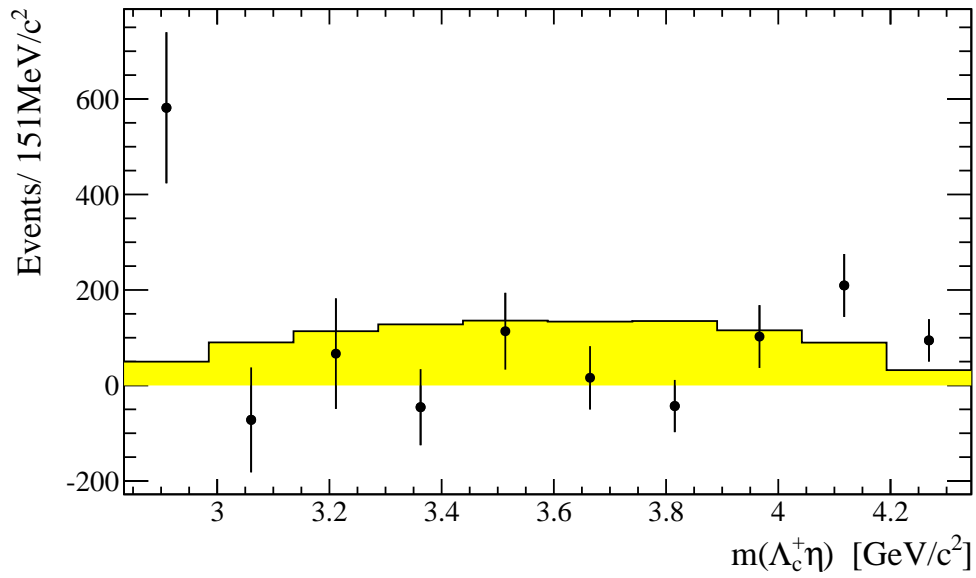


Figure 3.27: Efficiency corrected distribution of sideband subtracted signal data events (data points) and phase space generated MC signal events (histogram) for $m(\Lambda_c^+ \eta)$; scaled to the same integral.

4. Results and Conclusions

In this chapter all measured branching fractions will be summarized and compared with each other and theoretical predictions using the isospin of the final state. In the end we will make predictions for the branching fraction of other decay modes using the results we found.

For all ratios we calculate here in this chapter, the uncertainty on the branching fraction of the Λ_c^+ cancel out. When we compare the branching fractions of the \bar{B}^0 decay modes with the π^0 and η in the final state also some systematics cancel out.

4.1 Comparison of branching fractions

4.1.1 Measured branching fractions

We have observed the decay $\bar{B}^0 \rightarrow \Lambda_c^+ \bar{p} \pi^0$ for the first time and measured the branching fraction as:

$$\mathcal{B}(\bar{B}^0 \rightarrow \Lambda_c^+ \bar{p} \pi^0) = (1.94 \pm 0.17 \pm 0.14 \pm 0.50) \times 10^{-4}, \quad (4.1)$$

where the uncertainties are statistical, systematic, and from the Λ_c^+ branching fraction, $\Lambda_c^+ \rightarrow p K^- \pi^+$. For the resonant subchannel we calculate a 90% C.L. Bayesian upper limit of

$$\mathcal{B}(\bar{B}^0 \rightarrow \Sigma_c^+(2455) \bar{p}) \times \mathcal{B}(\Lambda_c^+ \rightarrow K^- p \pi^+) < 1.5 \times 10^{-6}. \quad (4.2)$$

We also found evidence for the decay $\bar{B}^0 \rightarrow \Lambda_c^+ \bar{p} \eta$ and measured the branching fraction as:

$$\mathcal{B}(\bar{B}^0 \rightarrow \Lambda_c^+ \bar{p} \eta) = (0.94 \pm 0.28 \pm 0.05 \pm 0.24) \times 10^{-4}, \quad (4.3)$$

where the uncertainties are statistical, systematic, and from the Λ_c^+ branching fraction, $\Lambda_c^+ \rightarrow p K^- \pi^+$.

4.1.2 Ratio of branching fractions

The ratio of the partial decay width measured here for the decay mode $\bar{B}^0 \rightarrow \Lambda_c^+ \bar{p} \pi^0$ to the *BABAR* measurement of the decay $B^- \rightarrow \Lambda_c^+ \bar{p} \pi^-$ [2] is

$$\frac{\Gamma(\bar{B}^0 \rightarrow \Lambda_c^+ \bar{p} \pi^0)}{\Gamma(B^- \rightarrow \Lambda_c^+ \bar{p} \pi^-)} = \frac{\mathcal{B}(\bar{B}^0 \rightarrow \Lambda_c^+ \bar{p} \pi^0)}{\mathcal{B}(B^- \rightarrow \Lambda_c^+ \bar{p} \pi^-)} \times \frac{\tau_{B^-}}{\tau_{\bar{B}^0}} = 0.62 \pm 0.07, \quad (4.4)$$

where τ_{B^-} and $\tau_{\bar{B}^0}$ are the lifetimes of the B mesons. This ratio is consistent with the isospin expectation of $2/3$ (eq. (1.1)). Given that we don't have evidence for a $\bar{B}^0 \rightarrow \Sigma_c^+ \bar{p}$ contribution, we also compare our $\bar{B}^0 \rightarrow \Lambda_c^+ \bar{p} \pi^0$ measurement with only the non-resonant contribution to the $B^- \rightarrow \Lambda_c^+ \bar{p} \pi^-$ decay. We find

$$\frac{\mathcal{B}(\bar{B}^0 \rightarrow \Lambda_c^+ \bar{p} \pi^0)}{\mathcal{B}(B^- \rightarrow \Lambda_c^+ \bar{p} \pi^-)_{\text{nonresonant}}} \times \frac{\tau_{B^-}}{\tau_{\bar{B}^0}} = 0.81 \pm 0.11, \quad (4.5)$$

which is within two standard deviations consistent with the isospin expectation of $2/3$. The 90% C.L. Bayesian upper limit for the ratio of the branching fractions $\mathcal{B}(\bar{B}^0 \rightarrow \Sigma_c^+(2455) \bar{p})$ and $\mathcal{B}(B^- \rightarrow \Sigma_c^0(2455) \bar{p})$ [2] is

$$\frac{\mathcal{B}(\bar{B}^0 \rightarrow \Sigma_c^+(2455) \bar{p})}{\mathcal{B}(B^- \rightarrow \Sigma_c^0(2455) \bar{p})} \times \frac{\tau_{B^-}}{\tau_{\bar{B}^0}} < 0.73, \quad (4.6)$$

which we compute by integrating the likelihood profile for the ratio of branching fractions over the positive range. It is also consistent with the isospin expectation of $2/3$.

The ratio of the partial decay width measured here for the \bar{B}^0 decay modes with a π^0 and η in the final state is

$$\frac{\Gamma(\bar{B}^0 \rightarrow \Lambda_c^+ \bar{p} \pi^0)}{\Gamma(\bar{B}^0 \rightarrow \Lambda_c^+ \bar{p} \eta)} = \frac{\mathcal{B}(\bar{B}^0 \rightarrow \Lambda_c^+ \bar{p} \pi^0)}{\mathcal{B}(\bar{B}^0 \rightarrow \Lambda_c^+ \bar{p} \eta)} = 2.06 \pm 0.65, \quad (4.7)$$

which is not consistent with the isospin expectation of $1/2$ we found in eq. (1.2).

The decay $\bar{B}^0 \rightarrow \Lambda_c^+ \bar{p} \pi^0$ could have two different isospins of the final state, $I = 1/2$ and $I = 3/2$, while the decay mode $B^- \rightarrow \Lambda_c^+ \bar{p} \pi^-$ has only $I = 3/2$ and the decay mode $\bar{B}^0 \rightarrow \Lambda_c^+ \bar{p} \eta$ only $I = 1/2$. We found in eq. (4.4) that the measured ratio is in a good agreement with the isospin expectation assuming that the final state of the decay $\bar{B}^0 \rightarrow \Lambda_c^+ \bar{p} \pi^0$ has always $I = 3/2$. But then of course the relation for the isospin expectation of $I = 1/2$ for the final state can not be fulfilled. But on the other hand we don't have seen the decay mode $\bar{B}^0 \rightarrow \Sigma_c^+(2455) \bar{p}$ and the ratio we calculated in eq. (4.5) is within the uncertainty of one standard deviation not consistent with our prediction in eq. (1.1). And that we have also found the decay mode $\bar{B}^0 \rightarrow \Lambda_c^+ \bar{p} \eta$ means, that there should also be a $I = 1/2$ component. In this case the value of both ratios in eq. (4.5) and eq. (4.7) must be too high compared with eq. (1.1) and eq. (1.2). But the good agreement between the measurement and the expectation for $I = 3/2$ also means that the dominant decay mechanism for $\bar{B}^0 \rightarrow \Lambda_c^+ \bar{p} \pi^0$ and $B^- \rightarrow \Lambda_c^+ \bar{p} \pi^-$ are the same. This could mean that the decay mechanism described by the diagram in fig. 1.7 could have a minor contribution to the decay $B^- \rightarrow \Lambda_c^+ \bar{p} \pi^-$.

4.1.3 Predictions

Because we found $\bar{B}^0 \rightarrow \Lambda_c^+ \bar{p} \eta$ there should be a $I = 1/2$ component for $\bar{B}^0 \rightarrow \Lambda_c^+ \pi^0$, too. We can also use eq. (1.1) and eq. (1.2) to calculate the different isospin components of the branching fraction $\mathcal{B}(\bar{B}^0 \rightarrow \Lambda_c^+ \bar{p} \pi^0)$. If we do so for the $I = 3/2$ component we find

$$\mathcal{B}(\bar{B}^0 \rightarrow \Lambda_c^+ \bar{p} \pi^0)_{I=3/2} = \frac{2}{3} \times \mathcal{B}(B^- \rightarrow \Lambda_c^+ \bar{p} \pi^-) \times \frac{\tau_{\bar{B}^0}}{\tau_{B^-}} = (1.60 \pm 0.13) \times 10^{-4} \quad (4.8)$$

and for the $I = 1/2$ component

$$\mathcal{B}(\bar{B}^0 \rightarrow \Lambda_c^+ \bar{p} \pi^0)_{I=1/2} = \frac{1}{2} \times \mathcal{B}(\bar{B}^0 \rightarrow \Lambda_c^+ \bar{p} \eta) = (0.47 \pm 0.14) \times 10^{-4}, \quad (4.9)$$

where the uncertainties don't include the uncertainty on $\mathcal{B}(\Lambda_c^+ \rightarrow p K^- \pi^+)$. Combining both isospin components we expect for the whole branching fraction

$$\mathcal{B}(\bar{B}^0 \rightarrow \Lambda_c^+ \bar{p} \pi^0) = \mathcal{B}(\bar{B}^0 \rightarrow \Lambda_c^+ \bar{p} \pi^0)_{I=3/2} + \mathcal{B}(\bar{B}^0 \rightarrow \Lambda_c^+ \bar{p} \pi^0)_{I=1/2} = (2.07 \pm 0.19) \times 10^{-4} \quad (4.10)$$

which is consistent with our direct measurement.

We can also use our direct measurement to predict the $I = 3/2$ component and the branching fraction for $B^- \rightarrow \Lambda_c^+ \bar{p} \pi^-$ if only the same Feynman diagrams would contribute. Using eq. (4.1) together with eq. (4.9) we find

$$\mathcal{B}_{I=3/2} = \mathcal{B}(\bar{B}^0 \rightarrow \Lambda_c^+ \bar{p} \pi^0) - \mathcal{B}(\bar{B}^0 \rightarrow \Lambda_c^+ \bar{p} \pi^0)_{I=1/2} = (1.47 \pm 0.25) \times 10^{-4} \quad (4.11)$$

which is the $I = 3/2$ component of our measured branching fraction for $\bar{B}^0 \rightarrow \Lambda_c^+ \bar{p} \pi^0$. Together with eq. (1.1) we can now predict the non-resonant branching fraction $\mathcal{B}(B^- \rightarrow \Lambda_c^+ \bar{p} \pi^-)$ to be

$$\mathcal{B}_{\text{predict.}}(B^- \rightarrow \Lambda_c^+ \bar{p} \pi^-)_{\text{nonresonant}} = \frac{3}{2} \times \mathcal{B}_{I=3/2} \times \frac{\tau_{B^-}}{\tau_{\bar{B}^0}} = (2.37 \pm 0.40) \times 10^{-4} \quad (4.12)$$

where we don't include the uncertainty on $\mathcal{B}(\Lambda_c^+ p K^- \pi^+)$ again.

If there are additional Feynman diagrams contributing to only one of both decay modes, there could be a difference in the predicted and measured branching fraction. For the decay $B^- \rightarrow \Lambda_c^+ \bar{p} \pi^-$ there is only one additional diagram, fig. 1.7. We can use the difference of the measured non-resonant branching fraction $\mathcal{B}(B^- \rightarrow \Lambda_c^+ \bar{p} \pi^-)_{\text{nonresonant}} = (2.57 \pm 0.21) \times 10^{-4}$ [2] and eq. (4.12) to make a prediction of the component where the π^- is created out of the W^- (fig. 1.7) to be

$$\mathcal{B}_{\text{ext}} = (0.20 \pm 0.45) \times 10^{-4} \quad (4.13)$$

which is consistent with zero and with our previous expectation that this diagram has only a very minor contribution to the whole branching fraction. This expectation isn't very strong but can be proved by analyzing decay modes like $B^- \rightarrow \Lambda_c^+ \bar{p} e \bar{\nu}_e$ or $B^- \rightarrow D_s^- \Lambda_c^+ \bar{p}$ for which fig. 1.7 is the only contributing diagram. There is also another diagram contribution to $B^- \rightarrow D_s^- \Lambda_c^+ \bar{p}$, but it needs the creation of a $c\bar{c}$ out of the vacuum which is expected to be suppressed.

From our prediction of the branching fraction \mathcal{B}_{ext} we can estimate an upper limit for the decay modes $B^- \rightarrow \Lambda_c^+ \bar{p} e^- \bar{\nu}_e$ and $B^- \rightarrow D_s^- \Lambda_c^+ \bar{p}$. An Bayesian 90% C.L. upper limit can be calculated assuming the probability of the number of signal events is Gaussian distributed around the mean of 0.20×10^{-4} with $\sigma = 0.45 \times 10^{-4}$ and we find $\mathcal{B}_{\text{UL}} < 0.88 \times 10^{-4}$. If we don't take the different mass of the D_s^- and π^- into account, we would expect for the branching fraction $\mathcal{B}(B^- \rightarrow \Lambda_c^+ \bar{p} D_s^-) < 0.88 \times 10^{-4}$.

To get an estimate for the semi-leptonic decay mode we can use τ decays to get an idea about the ratio of the π^- and e coming out of the W^- . For the ratio $\Gamma(\tau \rightarrow e^- \bar{\nu}_e \nu_\tau) / \Gamma(\tau \rightarrow \pi^- \nu_\tau)$ we find ~ 1.6 which leads to an expected branching fraction of $B^- \rightarrow \Lambda_c^+ \bar{p} e^- \tau_{e^-} < 1.4 \times 10^{-4}$.

4.2 Conclusion and Outlook

We have observed the decay $\bar{B}^0 \rightarrow \Lambda_c^+ \bar{p} \pi^0$ for the first time, measured the branching fraction and studied the three possible two-body invariant mass distributions. We have not seen possible Σ_c^+ resonances and calculated an upper limit for the branching fraction $\mathcal{B}(\bar{B}^0 \rightarrow \Sigma_c^+(2455) \bar{p})$. We have observed an mass enhancement at threshold for $m(\Lambda_c^+ \bar{p})$ like it is seen in many other processes with baryons in the final state. We have also found evidence for the decay $\bar{B}^0 \rightarrow \Lambda_c^+ \bar{p} \eta$ and calculated the branching fraction, too. We have also studied the possible two-body mass distributions. For this decay there is no enhancement at threshold for $m(\Lambda_c^+ \bar{p})$ found which could be due to different decay mechanism.

We compared the branching fraction for the two studied decay modes and the *BABAR* measurement of $B^- \rightarrow \Lambda_c^+ \bar{p} \pi^-$ using isospin relations. We find that the weak interaction also creates the final state with an isospin $I = 1/2$, although $I = 3/2$ is preferred for the decay mode $\bar{B}^0 \rightarrow \Lambda_c^+ \bar{p} \pi^0$. Moreover, we found that comparing the whole branching fraction of the measured decay mode with the π^0 in the final state and the non-resonant branching fraction for the decay mode with the π^- in the final state is a good agreement with the isospin expectations. From this we expect that the process described by fig. 1.7 has only a minor contribution to $\mathcal{B}(B^- \rightarrow \Lambda_c^+ \bar{p} \pi^-)$. Using this argument we gave an expectation for the branching fraction of the semi-leptonic decay mode and the decay of the \bar{B}^0 to $\Lambda_c^+ \bar{p} D_s^-$. Both expectations for the branching fraction should be able to prove with the data of the current B factories, *BABAR* and Belle, or at least at the LHCb.

To get an better idea of the decay mechanism which leads to the creation of baryons we have to study much more baryonic decay modes. The best would be to study different modes for which only one kind of diagram contributes and compare it with other known decay modes. Besides the semi-leptonic decay mode and the one with the D_s^- in the final state, one possible decay mode would be $\bar{B}^0 \rightarrow \Sigma_c^{++} \bar{\Sigma}^+ K^-$ for which only a diagram like fig. 1.8 is possible. This will be a task for analyses at LHCb and the upcoming experiments, like SuperB and Belle II.

Bibliography

- [1] B. Povh, K. Rith, C. Scholz, and F. Z. translated by Martin Lavelle, *Particles and nuclei: an introduction to the physical concepts*. Springer-Verlag GmbH, sixth ed., 2008.
- [2] **BABAR** Collaboration, B. Aubert *et al.*, “Measurements of $\mathcal{B}(\bar{B}^0 \rightarrow \Lambda_c^+ \bar{p})$ and $\mathcal{B}(B^- \rightarrow \Lambda_c^+ \bar{p} \pi^-)$ and Studies of $\Lambda_c^+ \pi^-$ Resonances,” *Phys. Rev.* **D78** (2008) 112003, [arXiv:0807.4974](#) [hep-ex].
- [3] **Particle Data Group** Collaboration, K. Nakamura *et al.*, “Review of particle physics,” *J. Phys.* **G37** (2010) 075021.
- [4] <http://www-public.slac.stanford.edu/babar/>.
- [5] **BABAR** Collaboration, B. Aubert *et al.*, “The BaBar detector,” *Nucl.Instrum.Meth.* **A479** (2002) 1–116, [arXiv:hep-ex/0105044](#) [hep-ex].
- [6] **BABAR** Collaboration, B. Aubert *et al.*, “Observation of the decay $\bar{B}^0 \rightarrow \Lambda_c^+ \bar{p} \pi^0$,” *Phys. Rev.* **D82** (2010) 031102, [arXiv:1007.1370](#) [hep-ex].
- [7] **CLEO** Collaboration, X. Fu *et al.*, “Observation of exclusive B decays to final states containing a charmed baryon,” *Phys. Rev. Lett.* **79** (1997) 3125–3129.
- [8] **ARGUS** Collaboration, H. Albrecht *et al.*, “SEARCH FOR HADRONIC b \rightarrow u DECAYS,” *Phys. Lett.* **B241** (1990) 278–282.
- [9] **BELLE** Collaboration, Y. J. Lee *et al.*, “Observation of $B^+ \rightarrow \Lambda$ anti-Lambda K^+ ,” *Phys. Rev. Lett.* **93** (2004) 211801, [arXiv:hep-ex/0406068](#).
- [10] **Belle** Collaboration, T. Medvedeva *et al.*, “Observation of the decay $\bar{B}^0 \rightarrow D_s^+ \Lambda \bar{p}$,” *Phys. Rev.* **D76** (2007) 051102, [arXiv:0704.2652](#) [hep-ex].
- [11] **BABAR** Collaboration, B. Aubert *et al.*, “Study of $e^+ e^- \rightarrow \Lambda$ anti-Lambda, Λ anti-Sigma0, Sigma0 anti-Sigma0 using initial state radiation with BABAR,” *Phys. Rev.* **D76** (2007) 092006, [arXiv:0709.1988](#) [hep-ex].
- [12] J. Gaiser, “Charmonium spectroscopy from radiative decays of the J/ψ and ψ' ,” SLAC-0255.

Danksagung

An dieser Stelle möchte ich mich bei allen bedanken, die mich während dieser Arbeit unterstützt haben.

Insbesondere möchte ich mich bei Priv.-Doz. Dr. Roland Waldi und Prof. Dr. Henning Schröder bedanken, welche mir die Möglichkeit gaben dieses Thema in der Rostocker Arbeitsgruppe zu studieren und diese Arbeit anzufertigen. Ebenfalls möchte ich mich für die hervorragende Betreuung und die vielen physikalischen Diskussionen bedanken, die mir oft neue Einblicke und Ideen verschafft haben.

Ich möchte mich auch bei allen Kollegen der Rostocker Arbeitsgruppe für Elementarteilchenphysik für die vielen Diskussionen und Hilfen in verschiedenen Dingen des täglichen Arbeitslebens bedanken.

Zu guter Letzt gilt mein besonderer Dank meiner Tochter Leonie, für ihre Geduld mit mir, vorallem während der letzten Phase dieser Arbeit.

